STEM CELLS AND DEVELOPMENT
Volume 26, Number 9, 2017

DOI: 10.1089/scd.2016.0262

Long-Term Exposure to Imatinib Mesylate Downregulates Hippo Pathway and Activates YAP in a Model of Chronic Myelogenous Leukemia

Anna Chorzalska,[1] Javier Flores Kim,[1] Karim Roder,[2] Alexander Tepper,[1] Nagib Ahsan,[3] R. Shyama Prasad Rao,[4] Adam J. Olszewski,[5] Xiaoqing Yu,[6] Dmitry Terentyev,[2] John Morgan,[7] Diana O. Treaba,[8] Ting C. Zhao,[9] Olin Liang,[5,10] Philip A. Gruppuso,[11] and Patrycja M. Dubielecka[1]

Despite the success of tyrosine kinase inhibitor (TKI) therapy in chronic myelogenous leukemia (CML), leukemic stem/progenitor cells remain detectable even in the state of deep molecular remission. Mechanisms that allow them to persist despite continued kinase inhibition remain unclear. We have previously shown that prolonged exposure to imatinib mesylate (IM) results in dysregulation of Akt/Erk 1/2 signaling, upregulation of miR-181a, enhanced adhesiveness, and resistance to high IM. To characterize the molecular basis and reversibility of those effects, we applied gene and protein expression analysis, quantitative phosphoproteomics, and direct miR-181a inhibition to our cellular model of CML cells subjected to prolonged exposure to IM. Those cells demonstrated upregulation of pluripotency markers (*SOX2, SALL4*) and adhesion receptors (CD44, VLA-4, CXCR4), as well as downregulation of Hippo signaling and upregulation of transcription coactivator YAP. Furthermore, inhibition of miR-181a using a microRNA sponge inhibitor resulted in decreased transcription of *SOX2* and *SALL4*, decreased activation of YAP, and increased sensitivity to IM. Our findings indicate that long-term exposure to IM results in dysregulation of stem cell renewal–regulatory Hippo/YAP signaling, acquisition of expression of stem cell markers and that experimental interference with YAP activity may help to restore chemosensitivity to TKI.

Keywords: chemoresistance, Hippo pathway, YAP, tyrosine kinase inhibitor, leukemic stem cells, imatinib mesylate

Introduction

In the last decade, the use of tyrosine kinase inhibitor (TKI)-based therapy for the treatment of *BCR-ABL1*-dependent chronic myelogenous leukemia (CML) redefined this disease from recalcitrant cancer to a manageable, chronic disorder with life expectancy approaching that of the general population [1]. In the randomized CML-Study IV, progression-free and overall survival rates, after 10 years of treatment with imatinib mesylate (IM), reached 82% and 84%, respectively [2]. However, IM treatment requires continuous administration of the drug, with a 76% cumulative incidence of adverse reactions at 8 years. Even though the rate of molecular remission (MR) reaches 59–92%, leukemic

[1]Signal Transduction Laboratory, Division of Hematology/Oncology, Department of Medicine, Rhode Island Hospital, Warren Alpert Medical School, Brown University, Providence, Rhode Island.
[2]Division of Cardiology, Rhode Island Hospital, Warren Alpert Medical School, Brown University, Providence, Rhode Island.
[3]Division of Biology and Medicine, Brown University, Center for Cancer Research and Development Proteomics Core Facility, Rhode Island Hospital, Providence, Rhode Island.
[4]Division of Biostatistics and Bioinformatics Division, Yenepoya Research Center, Yenepoya University, Mangalore, India.
[5]Division of Hematology/Oncology, Department of Medicine, Rhode Island Hospital, Warren Alpert Medical School, Brown University, Providence, Rhode Island.
[6]Department of Biostatistics, Yale School of Public Health, New Haven, Connecticut.
[7]Flow Cytometry and Cell Sorting Core Facility, Roger Williams Medical Center, Providence, Rhode Island.
[8]Department of Pathology and Laboratory Medicine, Rhode Island Hospital, Warren Alpert Medical School, Brown University, Providence, Rhode Island.
[9]Cardiovascular Laboratory, Department of Surgery, Roger Williams Medical Center, Boston University School of Medicine, Providence, Rhode Island.
[10]Department of Orthopedics, Warren Alpert Medical School, Brown University, Providence, Rhode Island.
[11]Department of Pediatrics, Brown University, Rhode Island Hospital, Providence, Rhode Island.

stem/progenitor cells (LS/PCs) are still detectable in the bone marrow of patients with deep MR defined as more than 4-log reduction of *BCR-ABL1* mRNA from a standardized baseline [3–5]. It is, therefore, not surprising that attempts to stop TKI treatment in patients with MR consistently show relapse rates of about 60% within the first 6 months after TKI discontinuation [6,7]. These findings indicate that measurement of *BCR-ABL1* transcript levels in the peripheral blood does not reflect eradication of the malignant clone, but also that the long-term effects of prolonged exposure to TKI at the molecular and stem cell levels are unknown. Since patients with CML are at present committed to life-long TKI therapy, understanding the long-term molecular effects of TKI treatment is of importance to the development of strategies to preserve and enhance chemosensitivity to these drugs.

Primitive cells that survive chemotherapy and contribute to tumor progression were first identified in human leukemia in 1960. CML stem cells were the first to be characterized as surviving in the presence of chemotherapeutics [8]. Detailed mechanistic studies of IM on stem cell survival have shown that *BCR-ABL1*-containing hematopoietic stem cells (HSCs) can survive in the absence of Bcr-Abl1 kinase activity [5,9]. These studies suggested that persistent LS/PCs, which are resistant to or unaffected by TKIs, may be responsible for relapse after TKI discontinuation [10]. This issue gains particular importance in the light of recent reports providing evidence that TKIs not only do not eliminate LS/PCs, but that prolonged TKI treatment may also paradoxically support their presence [11,12].

Signaling pathways that are essential for embryonic development and adult tissue homeostasis are often dysregulated in cancers. A population of rare cells termed cancer stem cells (CSCs) or cancer-initiating cells has been confirmed to exist in the majority of solid or hematological cancers. CSCs possess characteristics similar to normal stem cells, including the capacity for self-renewal and differentiation, which is thought to be responsible for sustained cancer growth and relapse [13,14]. Mounting evidence suggests that altered developmental signaling networks, such as those involving JAK/STAT, TGFβ, Wnt, Notch1, and Hedgehog, play an important role in maintaining CSCs and, thereby, the tumors themselves [15–17]. The Hippo pathway was recently identified as a mediator of developmental signals with a major role in organ homeostasis and stem-cell self-renewal [18]. It has also been found to have a role in carcinogenesis and CSCs biology [19,20]. More than 35 proteins have been identified in the human Hippo pathway. Upstream regulatory proteins control Yes-associated protein (YAP) and a transcriptional coactivator with PDZ-binding motif (TAZ or WW Domain-Containing Transcription Regulator 1 (WWTR1)) activity. This occurs through the regulation of the core kinase module, which consists of mammalian STE20-like protein kinase 1/2 (Mst1), Salvador homologue 1 (Sav1), Mob kinase activator 1A (Mob1A/B), and large tumor suppressor 1/2 (Lats1/2). Alternatively, upstream components, including tight/adherens junction proteins, members of the 14-3-3 family, scribble, or α catenin, can act directly on YAP and/or TAZ.

MicroRNAs are a class of small, noncoding RNAs about 22 nucleotides in length that are involved in the control of mRNA transcript stability [21]. Among 100 different miRNAs expressed in the hematopoietic system, the miR-181 family is the most highly conserved and the most preferentially expressed [22,23]. It includes six members encoded by three independent paralog precursors located on three separate chromosomes. The mature forms of miR-181a-1, miR-181a-2, miR-181b-1, and miR-181b-2 are identical. Together with miR-181c and miR-181d, they share the same 5′ seed sequence of 5′-AACAUUCA(A/U)(C/U)GCUGUCGGUG(A/G)GU-3′, indicating a high degree of functional redundancy between the members of the family. miR-181, which is strongly expressed in the thymus, is involved in T cell development, differentiation, and metabolic regulation [24–26]. It is also upregulated in mature B lymphocytes, suggesting a role in their differentiation [22]. Interestingly, miR-181 expression was also detected in lineage markers negative, undifferentiated progenitor cells [22], and in $CD34^+$ cells, where it is involved in the inhibition of differentiation [27]. The miR-181 family also plays a significant role in the enhancement of *OCT4*, *SOX2*, and *KLF4*-driven reprogramming and promotion of pluripotency [28], consistent with its engagement in stem cell renewal and maintenance. These findings are consistent with our observations made using IM-resistant CML cells that were generated by prolonged exposure to IM. Microarray analysis of these cells showed significant upregulation of miR-181a that correlated with increased levels of *NANOG* and *SOX2* [29]. However, the mechanism that links upregulation of miR-181a to increased expression of stem cell markers and IM resistance is unclear. In this study, we present evidence that long-term exposure to IM, while leading to a significant downregulation of Bcr-Abl1 protein level and its activity, results in inactivation of the Hippo pathway kinase module and upregulation of YAP, and that these changes correlate with increased expression of stem cell markers and acquired insensitivity to IM. Our observations are in agreement with a recent report showing increased levels of miR-181a in the plasma of CML patients who discontinued IM (STOP-IM group) [30]. In the present studies, we have observed that inhibition of miR-181a resulted in a decrease in YAP levels, an increase in its phosphorylation, and a modest but statistically significant increase in sensitivity to IM. Based on these data, we speculate that downregulation of the Hippo signaling kinase module and upregulation of YAP represents a new mechanism involved in maintenance of the LS/PC phenotype and leukemia recurrence after TKI discontinuation.

Materials and Methods

Cell lines and cell culture

The human chronic myeloid leukemia (CML) K562 cell line and its IM-resistant counterpart, clone K562-STI-R, were grown at 37°C, 5% CO_2 in RPMI 1640 medium (HyClone) supplemented with 10% fetal bovine serum (Corning cellgro) and 2 mM GlutaMAX (Gibco). The K562-STI-R cell line was established by culture in incremental concentrations of IM (Cayman Chemicals). The adhesive phenotype of these cells was originally noted at around the 20th passage. All experiments were performed on cells maintained for 60–75 passages in the presence of 0.6 μM IM. Adherent cells were grown to achieve no more than 70% confluency. About 70–80% of K562-STI-R cells remain adherent at any given time [29]. Cells in a logarithmic growth phase were used for all experiments. For IM

sensitivity experiments, cells were grown in 1, 10, 25, 50, or 100 μM IM. The number of apoptotic cells was evaluated by FACS using the Annexin V-FITC Early Apoptosis Detection Kit (#6592) from Cell Signaling Technology. Cell number was determined by counting in a hemocytometer using Trypan Blue dye exclusion.

Potassium EDTA-anticoagulated bone marrow cells were obtained from patients before initiation of IM therapy. $CD34^+$ cell-enriched populations were isolated before cryopreservation using the MicroBeads-Based Kit from Miltenyi (>85% purity). Informed consent was obtained in accordance with the Declaration of Helsinki and procedures were approved by the Institutional Research Board of the Rhode Island Hospital. For suspension cultures: $CD34^+$ cells were suspended in StemSpan Serum-Free Expansion Medium (SFEM II) supplemented with 10 ng/mL GM-CSF, 10 ng/mL G-CSF, 100 ng/mL SCF, 50 ng/mL LIF, 100 ng/mL MIP-1α, and 10 ng/mL hIL-6 (Stem Cell Technologies). A total of 5×10^4cells was then added to each well of a 24-well plate with or without 5 μM IM. Viable cell numbers were determined after 1 week of incubation by hemocytometer counts of Trypan Blue-excluding cells. For in vitro colony assays: 2×10^3 $CD34^+$ cells were plated in quadruplicate in methylcellulose-based medium with recombinant cytokines SCF, IL-3, EPO, and GM-CSF (H4434; Stem Cell Technologies) in the presence or absence of 5 μM of IM. Colonies derived from burst-forming units erythroid (BFU-E), multilineage granulopoietic, erythroid, macrophage, and megakaryocytic colony-forming units (CFU-GEMM), granulocyte–macrophage colony-forming units (CFU-GM), and macrophage colony-forming units (CFU-M) were scored in situ after 14 days of incubation using an inverted microscope.

Immunophenotyping

Cell samples were analyzed by FACS using a LSRII flow cytometer (Becton Dickinson). Data were analyzed with FACSDiva software v8.0 and FlowJo v10.1. Cell viability was assessed by Trypan Blue dye exclusion. In no case did apoptosis for either the K562 or K562-STI-R cells exceed 5%. The percentage of CML $CD34^+$ cells cultured for 1 week in the presence of 5 μM IM undergoing apoptosis was 39%. The following antibodies were used: human CD49d (9F10) APC, mouse/human CD44 (IM7) FITC, human NOTCH1 (MHN1-519) PE, human CD184 (12G5) PE, human CD34 (561) FITC (BioLegend), human CD133/1 (AC133) PE, human CD44 (DB105) APC, human CD24 (32D12) APC, and human CD34 (AC136) FITC (Miltenyi Biotec, Inc.). Isotype controls included mouse IgG1, κ (MOPC-21) APC, rat IgG2b, κ (RTK4530) FITC, mouse IgG1, κ (MOPC-21) PE, mouse IgG2a, κ (MOPC-173) PE, mouse IgG2a, κ (MOPC-173) FITC (BioLegend), and mouse IgG2a (S43.10) FITC (Miltenyi Biotec, Inc.). Unstained cells, isotype controls, and single-stained controls were used to determine gating.

Quantitative RT-PCR analysis

Total RNA from human K562 or K562-STI-R cells was purified using an RNeasy Mini Kit (Qiagen GmbH). Residual DNA was removed by on-column DNase I treatment (Qiagen GmbH). The iScript Advanced cDNA Synthesis Kit from Bio-Rad was used for reverse transcription according to the manufacturer's protocol. Relative levels of RNA were measured by quantitative real-time PCR using the C1000™ Thermal Cycler with CFX96™ Real-Time System (Bio-Rad) following the SsoAdvanced™ Universal SYBR® Green Supermix and Bio-Rad gene expression assay protocol. The following primers were designed for transcript quantification:

ABI1: For: 5′CTGGCACACTGTCGAGAACAA3′ and Rev: 5′CTTGGCGGTTTCTGAGTAGGA3′;
SALL4: 5′AGCACATCAACTCGGAGGAG3′ and Rev: 5′CATTCCCTGGGTGGTTCACTG′3′;
TDGF1: 5′TTTGAACTGGGATTAGTTGCCG3′ and Rev: 5′GGGGCCAAATGCTGTCATCT3′;
DNMT3B: For: 5′AGGGAAGACTCGATCCTCGTC3′ and Rev: 5′GTGTGTAGCTTAGCAGACTGG3′;
TAL1: For: 5′AGCCGGATGCCTTCCCTAT3′ and Rev: 5′GGGACCATCAGTAATCTCCATCT3′;
RUNX1: For: 5′CTGCCCATCGCTTTCAAGGT3′ and Rev: 5′GCCGAGTAGTTTTCATCATTGCC3′;
SOX2: For: 5′GCCGAGTGGAAACTTTTGTCG3′ and Rev: 5′GGCAGCGTGTACTTATCCTTCT3′;
NANOG: For: 5′TTTGTGGGCCTGAAGAAAACT3′ and Rev: 5′AGGGCTGTCCTGAATAAGCAG3′;
CITED2: For: 5′CCTAATGGGCGAGCACATACA3′ and Rev: 5′GGGGTAGGGGTGATGGTTGA3′;
POU5F1: For: 5′GACAGGGGGAGGGGAGGAGCTAG G3′ and Rev: 5′CTTCCCTCCAACCAGTTGCCCCAAAC3′;
AREG: For: 5′GTGGTGCTGTCGCTCTTGATA3′ and Rev: 5′CCCCAGAAAATGGTTCACGCT3′;
BIRC5: For: 5′AGGACCACCGCATCTCTACAT3′ and Rev: 5′AAGTCTGGCTCGTTCTCAGTG3′;
CTGF: For: 5′CAGCATGGACGTTCGTCTG3′ and Rev: 5′AACCACGGTTTGGTCCTTGG3′;
STAT3: For: 5′CAGCAGCTTGACACACGGTA3′ and Rev: 5′AAACACCAAAGTGGCATGTGA3′;
YAP1: For: 5′TAGCCCTGCGTAGCCAGTTA3′ and Rev: 5′TCATGCTTAGTCCACTGTCTGT3′;
WWTR1: For: 5′GATCCTGCCGGAGTCTTTCTT3′ and Rev: 5′CACGTCGTAGGACTGCTGG3′;
NOTCH1: For: 5′GAGGCGTGGCAGACTATGC3′ and Rev: 5′CTTGTACTCCGTCAGCGTGA3′';
CD44: For: 5′CTGCCGCTTTGCAGGTGTA3′ and Rev: 5′CATTGTGGGCAAGGTGCTATT3′;
S18: For: 5′GGGCGGAGATATGCTCATGTG3′ and Rev: 5′TCTGGGATCTTGTACTGTCGT3′;
ACTB: For: 5′CATGTACGTTGCTATCCAGGC3′ and Rev: 5′CTCCTTAATGTCACGCACGAT3′;
GAPDH: For: 5′TCATTGACCTCAACTACATGGTTT3′ and Rev: 5′GGCATGGACTGTGGTCATGAGTC3′.

All primers were purchased from IDT DNA. Results were normalized to the level of human *ACTB, S18*, or *GAPDH.* Human miR-181a, RNU19, and RNU6B were amplified using TaqMan Universal PCR Master Mix and miR-181a-specific and control TaqMan probes (Applied Biosystems by Life Technologies) [29]. Relative quantitation of gene expression was evaluated by CFX96 Real-Time System (Bio-Rad). Results were evaluated using Bio-Rad CFX manager.

Phosphopeptide enrichment and LC-MS/MS analysis

K562 or K452-STI-R cells in a logarithmic growth phase were harvested (five independently revived and grown cellular

clones per cell line) and lysed (8 M urea, 1 mM sodium orthovanadate, 20 mM HEPES, 2.5 mM sodium pyrophosphate, 1 mM β-glycerophosphate, pH 8.0, 20 min, 4°C), sonicated, and cleared by centrifugation (14,000 *g*, 15 min, 4°C). Protein concentration was measured (Pierce BCA Protein Assay; Thermo Fisher Scientific) and a total of 100 μg of protein per sample was subjected to trypsin digestion. The tryptic digested peptides were lyophilized and phosphopeptide enrichment was done using Titansphere Phos-TiO tips (GL Sciences) following the manufacturer's protocol with minor modifications. LC-MS/MS was performed on a fully automated proteomic technology platform [31]. Experiments were performed with an Agilent 1200 Series Quaternary HPLC system (Agilent Technologies) connected to a Q Exactive Plus Mass Spectrometer (Thermo Fisher Scientific).

Bioinformatics analysis

Peptide spectrum matching of MS/MS spectra of each file was searched against a human-specific database (UniProt; downloaded 2/1/2013) using MASCOT v. 2.4 (Matrix Science Ltd.). A concatenated database containing 144,156 ''target'' and ''decoy'' sequences was employed to estimate the false discovery rate (FDR). Msconvert from ProteoWizard (v. 3.0.5047), using default parameters and with the MS2Deisotope filter on, was employed to create peak lists for Mascot. Search parameters permitted variable modification of methionine oxidation (+15.9949 Da), and static modification of carbamidomethylation (+57.0215 Da) on cysteine. To identify the phosphoresidues' additional variable modification of phosphorylation (+79.9663 Da) on serine, threonine and tyrosine residues were included. Peptide assignments from the database search were filtered down to 1% FDR by a logistic spectral score, as previously described [32,33]. To validate the position of the phosphorylation sites, the Ascore algorithm [34] was applied and the reported phosphorylation site position reflected the top Ascore prediction.

Relative quantitation of the phosphopeptides

Relative quantitation of phosphopeptide abundance was performed through calculation of selected ion chromatogram (SIC) peak areas. Retention time alignment of individual replicate analyses was performed as previously described [35]. SIC peak areas were determined for every phosphopeptide that was identified by MS/MS. In the case of a missing MS/MS for a particular peptide in a particular replicate, the SIC peak area was calculated according to the peptide's isolated mass and retention time calculated from retention time alignment. A minimum SIC peak area equivalent to the typical spectral noise level of 1,000 was required of all data reported for label-free quantitation. Individual SIC peak areas were normalized to the peak area of the standard phosphopeptide DRVpYHPF that was added before phosphopeptide enrichment and reversed-phase elution into the mass spectrometer.

Proteomic result data analysis

Functional analysis of phosphoproteomics data was performed using MetaCore™ software suite. Volcano plot was calculated from the log 2 of the ratio of the fold change of each peptide peak area compared with the natural log of the *q*-value of each peptide.

Immunoblotting and immunofluorescence

Whole cell lysates were used in all experiments. Protein levels were equalized based on β-actin protein level. Western blotting was performed as described previously [29]. The following antibodies were used: rabbit polyclonal anti-Abi-1 #NB100-59845 (Novus Biologicals), mouse monoclonal anti-Abi-1 #D147-3 (MBL International Corporation), mouse monoclonal anti-SSH3BP1 [4E2] #ab11222 (Abcam), Mouse monoclonal anti-Abi1 (clone 2G8) unpublished (kind gift from L. Kotula, Upstate Medical University in Syracuse, NY), mouse monoclonal anti-c-Abl #OP20 (Calbiochem/Millipore), rabbit monoclonal phospho-anti-c-Abl (Tyr412) # 2865, rabbit polyclonal anti-Mst1 #3682, rabbit monoclonal anti-Sav1 #13301, rabbit monoclonal anti-Lats1 #3477, rabbit monoclonal anti-Mob1 #13730, rabbit monoclonal phospho-anti-YAP(S127) #1308, rabbit monoclonal phospho-anti-YAP(S397) #13619, mouse monoclonal anti-CrkL #3182, and rabbit polyclonal anti-phospho-CrkL (Tyr207) #3181 were from Cell Signaling Technology. Rabbit monoclonal anti-YAP/TAZ was from Abcam #ab52771. Mouse monoclonal anti-β-actin #A1978 was from Sigma-Aldrich. Peroxidase-conjugated AffiniPure goat anti-rabbit (H+L) and goat anti-mouse (H+L) were from Jackson ImmunoResearch Laboratories, Inc. Immunofluorescence was performed as described [36]; rabbit monoclonal anti-YAP/TAZ #ab52771 followed by goat anti-rabbit conjugated with AlexaFluor 555 were used, phalloidin conjugated with AlexaFluor 555 was used to visualize F-actin (Invitrogen). Confocal images were acquired with a Nikon C1si confocal (Nikon, Inc.) using diode lasers 402, 488, and 561. Serial optical sections were performed with EZ-C1 software (Nikon, Inc.). Z series sections were collected at 0.2 μm with a 60× PlanApo objective and scan zoom of 2. Images were processed and projected in Elements software (Nikon, Inc.).

FIG. 1. *NOTCH1, STAT3*, and *CD44* expression in hematopoietic progenitor cells obtained from CML patients. **(A)** Affymetrix Human Genome U219 Array results for *NOTCH1, STAT3, CD44* expression were analyzed. Analyses were carried out on $CD34^+$ cells obtained from the bone marrow of CML patients at diagnosis ($n=6$, pre-IM) and 1 week after the initiation of therapy ($n=6$, post-IM; *top* three panels), and at diagnosis ($n=9$, pre-IM), and 4 weeks after initiation of therapy ($n=9$, post-IM; *lower* three panels). The following probe sets were evaluated using the deposited GEO GSE12211 and GSE33075 databases (GPL571 and GPL570 platforms, respectively). The status of expression of probes 218902_at for *NOTCH1*, 208991_at for *STAT3*, and 204489_s_at for *CD44* is presented as interquartile range and median of normalized, log-transformed raw data. *P*-values are denoted on the graphs. **(B)** Hematopoietic progenitor cells were obtained from CML patients ($n=3$) before initiation of TKI therapy. *NOTCH1, STAT3*, and *CD44* expression was determined on CML $CD34^+$ cells cultured with or without 5 μM IM for 1 week. Normalized expression relative to *ACTB* expressed as fold change, is presented. Samples were cultured and run in triplicate $^{**}P<0.01$. CML, chronic myelogenous leukemia; IM, imatinib mesylate.

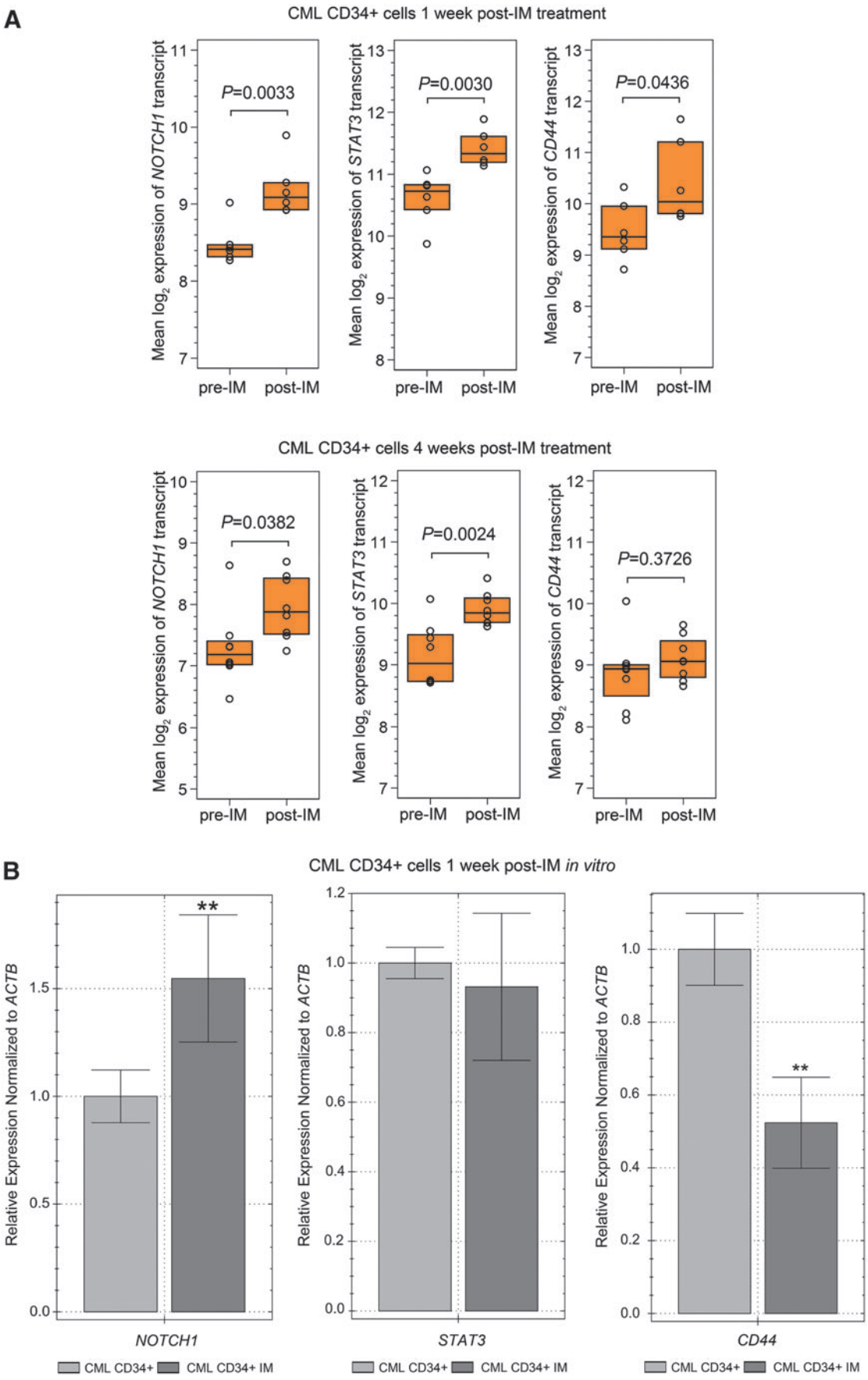
A
CML CD34+ cells 1 week post-IM treatment
Mean log2 expression of NOTCH1 transcript
P=0.0033
pre-IM
post-IM
Mean log2 expression of STAT3 transcript
P=0.0030
pre-IM
post-IM
Mean log2 expression of CD44 transcript
P=0.0436
pre-IM
post-IM
CML CD34+ cells 4 weeks post-IM treatment
Mean log2 expression of NOTCH1 transcript
P=0.0382
pre-IM
post-IM
Mean log2 expression of STAT3 transcript
P=0.0024
pre-IM
post-IM
Mean log2 expression of CD44 transcript
P=0.3726
pre-IM
post-IM
B
CML CD34+ cells 1 week post-IM in vitro
Relative Expression Normalized to ACTB
**
NOTCH1
CML CD34+
CML CD34+ IM
Relative Expression Normalized to ACTB
STAT3
CML CD34+
CML CD34+ IM
Relative Expression Normalized to ACTB
**
CD44
CML CD34+
CML CD34+ IM

MicroRNA sponge design

To construct the miR-181a sponge, oligonucleotides were designed to contain two miR-181a binding sites. Each binding site was composed of a 22-nucleotide long sequence complementary to the sequence of miR-181a. Each binding site contained a central mismatch at positions 11–14, in which the nucleotide at position 14 was deleted. The two miR-181a binding sites were separated by a sequence of four nucleotides (AATT). Control sponges were designed to have a scrambled sequence at positions 3–8, the region that corresponds to the miR-181a seed sequence. Sense and antisense oligomers were synthesized, PAGE purified at a 100 nmol scale, and phosphorylated at the 5′ ends. The oligomers had overhangs compatible with the restriction endonuclease SanDI. Complementary oligomer pairs were mixed in a 1:1 ratio and annealed. T4 ligase was used for oligomer duplexes ligation into multimers. Empty pcDNA3-SanDI or pcDNA3-SanDI-GFP mammalian expression vectors (kind gift from Dr. Kluiver, University Medical Center, The Netherlands) were digested with SanDI restriction endonuclease and dephosphorylated with alkaline phosphatase (Fermentas). T4 Ligase (New England BioLabs, Inc.) was used to ligate the multimers into the pcDNA3-SanDI or pcDNA3-SanDI-GFP. The number of oligomers ligated into the expression vector was verified in a digestion reaction using EcoRI and BamHI restriction endonucleases. Vectors containing 8, 6, and 4 oligomer duplexes for control or miR-181a sponge (16-, 12-, 8-mers) were sequenced and tested for the effect on miR-181a. Vectors containing octamer control or octamer miR-181a sponge were selected for subsequent experiments.

Electroporation

Vectors used for electroporation were purified using the EndoFree Plasmid Maxi Kit (Qiagen GmbH). DNA purity and integrity were determined spectroscopically ($OD_{260nm}/OD_{280nm} = 1.90–2.0$), ($OD_{260nm}/OD_{230nm} > 2.00$). DNA electroporation was performed with Neon® Transfection System (Life Technology) according to optimized manufacturer's instruction. After electroporation, cells were seeded into 10-cm plates with 10 mL of prewarmed RPMI 1640 containing IM and incubated at 37°C in a humidified CO_2 incubator for the next 24 h.

Statistical analyses

We performed statistical analyses using two-tailed unpaired Student's *t*-test. We considered values of $P < 0.05$ to be statistically significant ($^*P < 0.05$, $^{**}P < 0.01$, and $^{***}P < 0.001$). For phosphoproteomic analyses *P*-values were calculated from five replicates. To select phosphopeptides that show statistically significant change in abundance between K562-STI-R cells and K562 cell lines, two-tailed unpaired Student's *t*-test and *q*-values for multiple hypothesis tests were calculated based on the determined *P*-values using the R package QVALUE as previously described [37].

Results

Exposure to IM results in increased expression of stem cell markers and acquired insensitivity to IM

Recent reports suggest that TKI therapy not only fails to eliminate LS/PCs, but that it may also actually support their presence and contribute to upregulation of certain stem cell markers [11,12]. To determine the effect of IM on the genes that are associated with the stem cell and CSC phenotypes (*SALL4*, *OCT4*, *SOX2*, *NANOG*, *CD44*, *CD133*, and *STAT3*), we analyzed published microarray data that had examined gene expression in CML $CD34^+$ cells isolated from the bone marrow at diagnosis and after IM initiation. Two data sets were analyzed: NCBI/GEO/GSE12211, includes data on six patients from whom samples were obtained before IM initiation, and six patients from whom samples were obtained 7 days after IM initiation [38]; NCBI/GEO/GSE33075, includes nine patients from whom samples were obtained before IM initiation and nine patients from whom samples were obtained 4 weeks after imatinib initiation [39]. In both studies, patients received a standard IM daily dose of 400 mg. Our analysis of these data (Fig. 1A) showed a significant increase in transcripts for *NOTCH1, STAT3*, and *CD44* 1 and 4 weeks following initiation of IM therapy. This suggested that both short and prolonged exposure to IM may result in upregulation of gene transcripts associated with the CSC phenotype.

We also assessed the direct effect of IM on the expression of *NOTCH1*, *STAT3*, and *CD44* in the CML $CD34^+$ cells isolated from the bone marrow of CML patients prior initiation of IM therapy and cultured in vitro for 1 week in 5 μM IM in serum-free expansion medium supplemented with cytokines. The presence of 5 μM of IM for 1 week resulted in a five-fold decrease in CML $CD34^+$ cell number (Supplementary Fig. S1A; Supplementary Data are available online at www.liebertpub.com/scd) and a five-fold decrease in the colony formation capacity of CML $CD34^+$ cells (Supplementary Fig. S1B). Thirty-nine percent of surviving CML $CD34^+$ cells were apoptotic. These observations are in line with previously described findings [5,40,41]. One week-long exposure to IM also resulted in increased expression of *NOTCH1* (Fig. 1B), in agreement with findings presented on Fig. 1A. Notably, transcript levels of *STAT3* remained unaffected, whereas mRNA levels of *CD44* were significantly reduced (Fig. 1B). These data indicate that exposure to IM may directly affect expression of stem cell markers.

We extended these observations to our established cellular model of long-term exposure to IM. This model, the K562-STI-R cell line, was established by culturing K562 CML cells in concentrations of IM that were increased until selection resulted in cells that were viable in the presence of 10 μM IM. K562-STI-R cells were maintained in 0.6 μM IM for 60–75 passages; 70–80% of these cells persisted in being adherent. K562-STI-R cells display significant downregulation of Bcr-Abl1 protein levels and activity (Supplementary Fig. S2 and also [29]). We examined the K562-STI-R expression pattern of the pluripotency markers *OCT4 (POU5F1)*, *NANOG*, *SOX2*, *TDGF1*, and *DNMT3*, and of the HSC markers *SALL4*, *CITED2* (regulators of human hematopoiesis), and *TAL1 (*regulator of HSC quiescence*). ACTB*, *S18*, and *GAPDH* were used as controls. Results (Fig. 2A) showed upregulation of *SOX2* and *SALL4* in the K562-STI-R cells. *NANOG*, *CITED2*, *DNMT3A*, and *TAL1* were downregulated (Supplementary Fig. S3A, B). Since both *SOX2* and *SALL4* are well-established regulators of cell fate during development whose upregulation is associated with maintenance of CSCs [42,43], we interpreted our data as

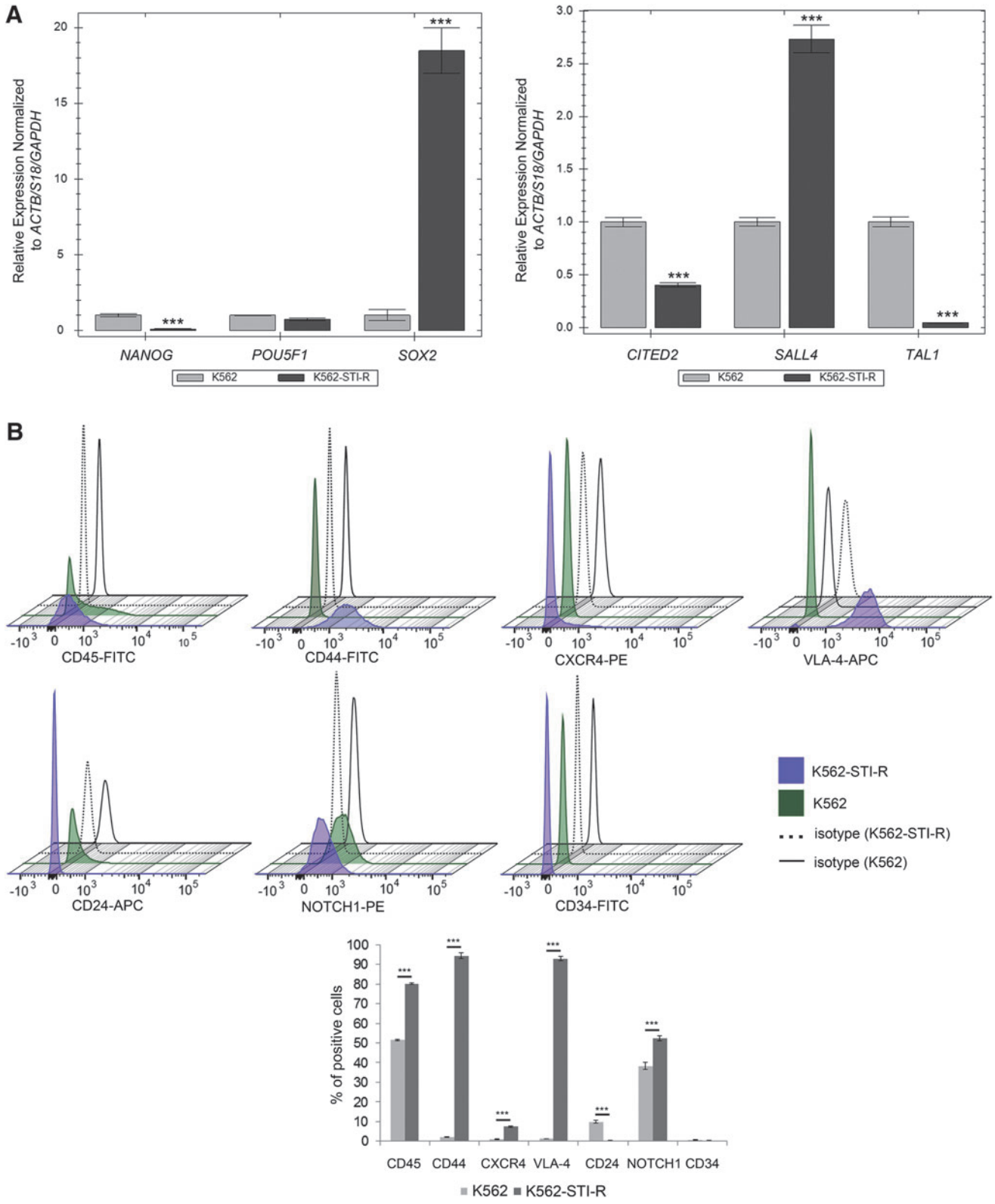

FIG. 2. Stem cell markers and sensitivity to IM in K562 and IM-resistant K562-STI-R cells. **(A)** Expression of *NANOG, POU5F1, SOX2, CITED2, SALL4*, *and TAL1* was determined in K562 or IM-resistant K562-STI-R cells. Data represent normalized expression relative to *ACTB*, *S18*, and *GAPDH*. Samples were run in triplicate. Representative data from three independent analyses are shown. ***$P < 0.001$ **(B)** Expression of CD45, CD44, CXCR4, VLA-4, CD24, NOTCH1, and CD34 was determined by FACS in K562 and K562-STI-R cells. 3D histograms and a bar graph summary of the quantitative results are presented. Representative data from three independent analyses are shown. ***$P < 0.001$ **(C)** Coexpression of CD44 and CD24 by FACS was determined for K562 and K562-STI-R cells. Analyses were performed in quadruplicate. Representative data are shown. **(D)** FACS analyses were used to determine the percentage of apoptotic cells in a population of K562 and K562-STI-R cells subjected to incremental concentrations of IM for 24 h. The percent Annexin V-FITC-positive cells was determined. Representative data from three independent analyses are shown *$P < 0.05$.

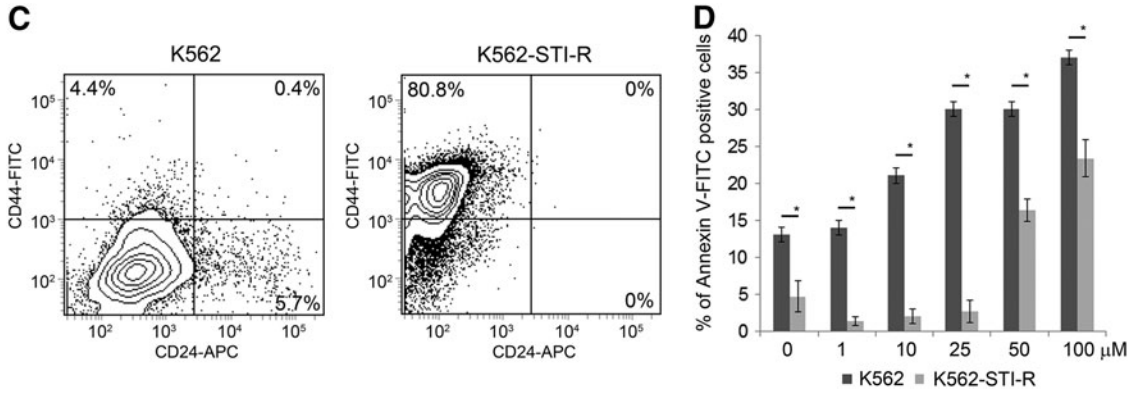

FIG. 2. (Continued).

indicating that long-term exposure to IM may promote the stem cell phenotype and acquisition of a CSC phenotype.

We then examined the expression of adhesion receptors that regulate interactions between HSCs and their microenvironment, and are associated with adhesion-mediated drug resistance and the CSC phenotype [44]. These include CD34, CXCR4 (C-X-C chemokine receptor type 4), VLA-4 (Very Late Antigen 4, CD49f), NOTCH1, CD44, CD24, and CD133. We found a significant upregulation of CD44 and VLA-4, a modest increase in expression of CXCR4 and NOTCH1, and a modest decrease in the expression of CD24 (Fig. 2B). The $CD44^{hi}/CD24^{low}$ phenotype, present in the K562-STI-R cells (Fig. 2C), is associated with the CSC phenotype [45,46]. These results indicated that long-term exposure to IM induces upregulation of adhesion receptors that may contribute to an increase in adhesion.

Finally, we evaluated the sensitivity of K562-STI-R cells to incremental concentrations of IM. K562-STI-R cells that overexpressed genetic and surface markers associated with stem cell potential and the adhesive phenotype showed significant resistance to IM treatment. These cells were able to withstand very high concentrations of the drug, with an increase in apoptotic cells occurring only at IM concentrations in excess of 25 μM (Fig. 2D). These data indicate that cells exposed to long-term IM treatment display a high degree of resistance to IM and upregulate genetic (*SOX2*, *SALL4*) and surface (CD44, VLA-4, CXCR4) markers associated with the stem cell phenotype.

Long-term exposure to IM results in the inhibition of Hippo signaling kinase module and increased YAP activity

To investigate the signaling pathways involved in the phenotype associated with long-term exposure to IM, we performed label-free, quantitative phosphoproteomic analysis of K562 and K562-STI-R cells. For each cell type, a total of five biological replicates were analyzed using LC–MS/MS (experimental strategy presented in Supplementary Fig. S4). Using a 1% FDR, we quantified 4,807 unique phosphopeptides derived from 1,559 proteins. The complete list of the identified phosphopeptides subjected to quantitative analysis is presented in Supplementary Table S1. The pairwise analysis of replicate peak areas indicated a high degree of quantitative reproducibility between individual LC–MS runs used for label-free, intensity-based quantitation. Among all identified phosphopeptides, a total of 2,593 phosphopeptides representing 1,175 phosphoproteins showed a statistically significant difference between the two cell lines. Detection of significantly altered phosphopeptides was carried out by applying Student's *t*-test with a *q*-value correction for multiple comparisons. A volcano plot representing the relationship between fold change and *q*-value (Fig. 3A) illustrates that among 36.9% of identified phosphopeptides with an absolute fold change greater than 2, 88.3% of peptides showed lower abundance in the K562-STI-R cells, whereas 11.7% showed higher peak abundance. We performed a functional analysis of the significantly different phosphopeptides using MetaCore software. The top five identified pathways included cell cycle (chromosome condensation), cytoskeleton remodeling, Erk1/2 signaling, transport (AVP regulation of aquaporin 2), and development (negative regulation of Hippo pathway and positive regulation of YAP/TAZ function) (Fig. 3B). Based on its potential role in the K562-STI-R phenotype that we observed, we focused on the Hippo pathway.

The list of top five identified pathways-associated phosphopeptides that differed in abundance in the K562-STI-R cells relative to K562 cells is presented in Table 1. In Fig. 3C, we present a schematic outline of the Hippo cascade, with phosphosites identified in our phosphoproteomic analysis highlighted. Immunoblotting for components of the Hippo pathway (Fig. 3D) showed significantly decreased expression levels of Lats1, Sav1, and Mob in the IM-resistant cells. This was associated with an increase in YAP protein levels and a marked reduction in the stoichiometry of phosphorylation of YAP on Ser 127 and Ser 397. Evaluation of the expression levels of YAP targets showed downregulation of *AREG* and *BIRC5* and upregulation of *CTGF* (Fig. 3E and Supplementary Fig. S5).

The human CML $CD34^+$ samples did not disclose changes in *YAP* or *WWTR1* (TAZ) expression after 1 week of IM treatment (GEO/GSE12211) [38], however an increase in *WWTR1(TAZ)* transcript levels was present in CML $CD34^+$ samples obtained after 4 weeks of IM administration (Fig. 4A) (GEO/GSE33075) [39]. In CML $CD34^+$ cells cultured in the presence of 5 μm of IM in vitro we observed a two-fold increase in transcript levels of both *YAP* and *WWTR1* after 1 week culture in the presence of the drug (Fig. 4B). We interpreted these data as indicating that exposure to IM results in

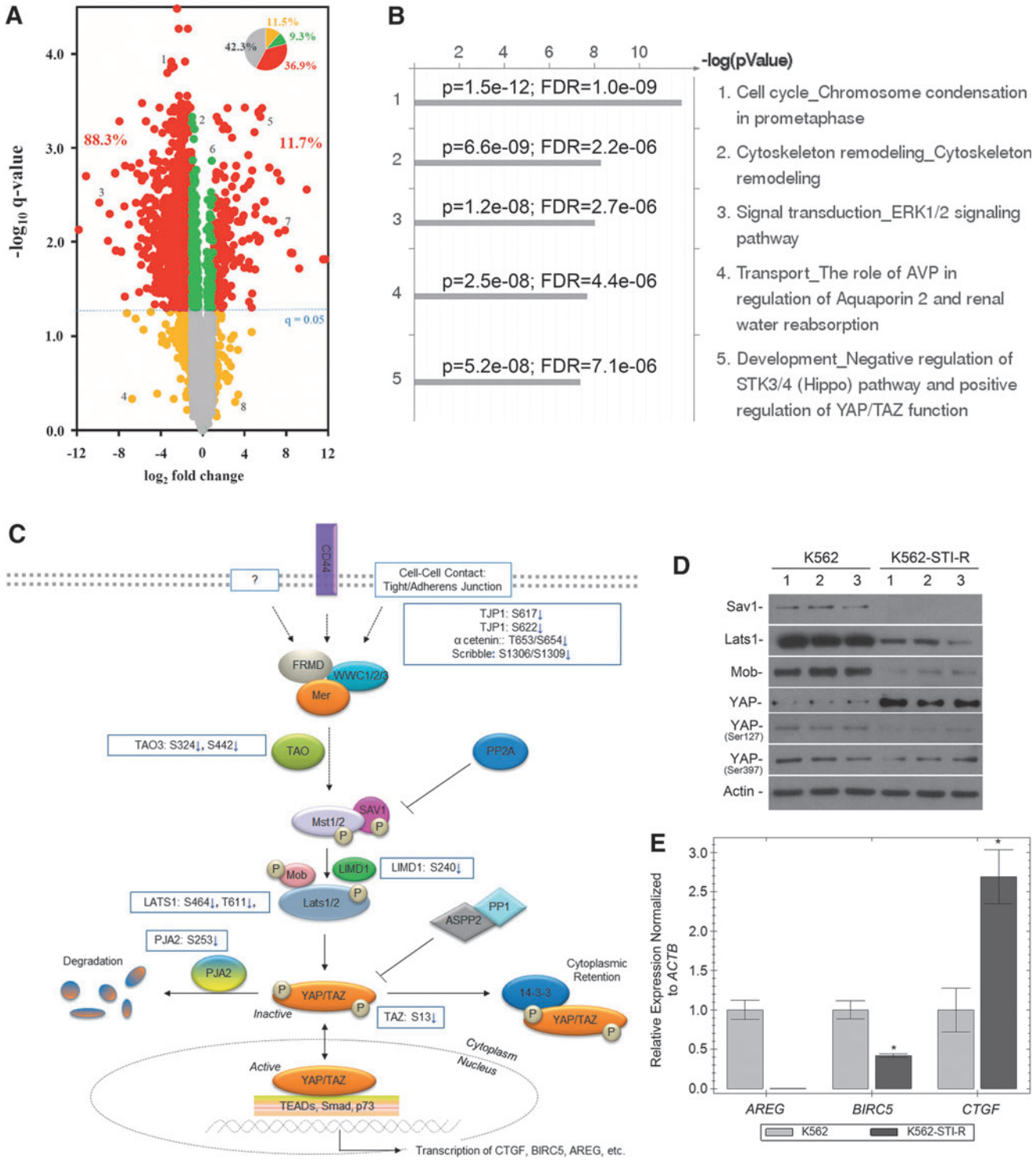

FIG. 3. Effect of long-term exposure to IM on the Hippo pathway and YAP. **(A)** Volcano plots showing fold change versus *q*-value of phosphopeptide peak areas were generated. Of the 4,807 unique phosphopeptides identified, 36.9% peptides (*red* in *inset* pie chart) showed a statistically significant ($q < 0.05$) difference and an absolute fold change greater than 2 comparing the K562-STI-R cells to control K562 cells. Within this group of significantly different peptides, 88.3% showed lower abundance in the K562-STI-R cells. **(B)** The five most highly scored pathways identified in K562-STI-R cells reflect the enrichment analysis of gene IDs corresponding to the proteins for which identified phosphopeptides showed statistically a significant ($q < 0.05$) fold change >2. **(C)** This schematic representation of Hippo/YAP cross-talk shows phosphosites that were significantly different in K562-STI-R cells versus control K562 cells. **(D)** Western blot analysis was performed on K562 and K562-STI-R whole cell lysates. Levels of Sav1, Lats1, Mob, and YAP along with phosphorylation of YAP on Ser127 and 397 were evaluated. Data from three independent, replicate cultures of each cell line representing three independent experiments are shown. **(E)** RT-PCR was performed to quantify *AREG, BIRC5*, and *CTGF* expression in K562 and IM-resistant K562-STI-R cells. Data are presented as normalized expression relative to *ACTB*. Samples were run in triplicate. Representative data from three independent analyses are shown $^*P < 0.05$.

TABLE 1. THE LIST OF PHOSPHOPEPTIDES ASSOCIATED WITH TOP FIVE PATHWAYS IDENTIFIED TO BE DYSREGULATED IN THE K562-STI-R RELATIVE TO K562 CELLS

Protein name	*Peptide sequence (*phosphorylated, #methionine oxidation)*	*Phosphorylation site (p-site)*	*Accession no. for p-site*	*Ratio K562-STI-R/K562*	*q-Values*	*Charge state*	*Gene symbol*	*HPRD accession*
Cell cycle—chromosome condensation in prometaphase								
Histone H1x	K.AGGSAALS*PSKK.R	S31*	HPRD:04151_1	0.019244966	3.83359E-05	2	*H1FX*	04151_1
Topoisomerase DNA II, beta	K.VVEAVNS*DS*DS*EFGIPK.K	S1517S1519S1521*	HPRD:00537_1	0.060399862	0.000632588	2	*TOP2B*	00537_1
Topoisomerase DNA II, beta	K.VVEAVNS*DS*DSEFGIPKK.T	S1517S1519*	HPRD:00537_1	0.11168151	4.40595E-06	3	*TOP2B*	00537_1
Inner centromere protein	R.AAAAAAAATMALAAPS* SPTPES*PTMLTK.K	S142S148*	HPRD:05103_1	0.134864416	0.000258977	3	*INCENP*	05103_2
Topoisomerase DNA II, beta	K.YFAES*DEEEDDVDFAMFN.-	S1608	HPRD:00537_1	0.157412811	0.040967043	2	*TOP2B*	00537_1
Topoisomerase DNA II, beta	K.SEDDSAKFDS*NEEDSA SVFSPSFGLK.Q	S1461*	HPRD:00537_1	0.168750517	0.005740955	3	*TOP2B*	00537_1
Cyclin B2	K.DLASPLIGRS*.-	S398	HPRD:04131_1	0.170492751	0.000897379	2	*CCNB2*	04131_1
Inner centromere protein	R.IAQVS*PGPR.D	S263*	HPRD:05103_1	0.192521701	4.99393E-06	2	*INCENP*	05103_2
Topoisomerase DNA II, beta	R.KAS*GS*ENEGDYNPGR.K	S1545S1547*	HPRD:00537_1	0.227852671	7.9002E-06	2	*TOP2B*	00537_1
H3 Histone, family 3B	K.S*TELLIR.K	S58	HPRD:03036_1	0.251507088	5.84008E-06	2	*H3F3B*	18825_1
CDC2	K.IGEGT*YGVVYK.G	T14*	HPRD:00302_1	0.254472604	0.000406451	3	*CDK1*	00446_1
Inner centromere protein	R.AAAAAAAATMALAAPSS* PTPES*PTMLTK.K	S143S148*	HPRD:05103_1	0.261545024	0.001363582	4	*INCENP*	05103_2
KARP 1 binding protein	R.ST*GS*ATSLASQGER.R	T628S630*	HPRD:17172_1	0.323005541	0.000253714	2	*CEP170*	17172_3
Chromosome condensation protein G	K.TLHCEGTEINS*DDEQE SKEVEETATAK.N	S674*	HPRD:12097_1	0.346120173	0.005823643	3	*NCAPG*	12097_1
KARP 1 binding protein	R.S*DSEATISR.S	S1165	HPRD:17172_1	0.35100536	3.89936E-05	2	*CEP170*	17172_3
KARP 1 binding protein	R.STGS*ATSLASQGER.R	S630*	HPRD:17172_1	0.36744914	0.000148779	2	*CEP170*	17172_3
Chromosome condensation protein G	K.LNLAQFLNEDLS*.-	S1015	HPRD:12097_1	0.382107906	0.009815237	2	*NCAPG*	12097_1
CDC2	K.IGEGT*Y*GVVYKGR.H	T14Y15*	HPRD:00302_1	0.411471675	0.002256503	3	*CDK1*	00302_2
CND2	R.LLAS*PSSR.S	S87	HPRD:03820_1	0.442434391	4.82902E-05	2	*NCAPH*	03820_1
Inner centromere protein	K.INPDNY*GMDLNS*DDST* DDEAHPR.K	Y818S824T828*	HPRD:05103_1	0.481723555	0.006483106	3	*INCENP*	05103_2
Non-SMC condensin II complex, subunit H2	K.ESRS*PQQSAALPR.R	S284*	HPRD:11783_1	0.677367739	0.003665133	3	*NCAPH2*	11783_3
Chromosome condensation protein G	R.CQT*AEADSES* DHEVPEPESEMK.M	T968S975*	HPRD:12097_1	0.679711752	0.020134351	3	*NCAPG*	12097_1
Chromosome condensation protein G	R.CQTAEADS*ES* DHEVPEPESEMK.M	S973S975*	HPRD:12097_1	0.679877906	0.020178793	3	*NCAPG*	12097_1
DNA topoisomerase II alpha	K.NENTEGS* PQEDGVELEGLKQR.L	S1247*	HPRD:00536_1	0.760612799	0.022737593	3	*TOP2A*	00536_1

(*continued*)

TABLE 1. (CONTINUED)

Protein name	*Peptide sequence (*phosphorylated, #methionine oxidation)*	*Phosphorylation site (p-site)*	*Accession no. for p-site*	*Ratio K562-STI-R/K562*	*q-Values*	*Charge state*	*Gene symbol*	*HPRD accession*
DNA topoisomerase II alpha	K.SVVS*DLEADDVK.G	S1377*	HPRD:00536_1	0.797929426	0.045978223	2	*TOP2A*	00536_1
Chromosome condensation-related SMC-associated protein 1	R.YQPLAS*TASDNDFVT*PEPR.R	S1330T1339*	HPRD:06472_1	2.062328833	0.011033288	3	*NCAPD2*	06472_1
Chromosome condensation-related SMC-associated protein 1	R.YQPLAST*ASDNDFVT*PEPR.R	T1331T1339*	HPRD:06472_1	2.067195121	0.01091227	3	*NCAPD2*	06472_1
Chromosome condensation-related SMC-associated protein 1	R.YQPLASTAS*DNDFVT*PEPR.R	S1333T1339*	HPRD:06472_1	2.06901788	0.010957473	3	*NCAPD2*	06472_1
Cytoskeleton remodeling								
Myosin heavy chain, nonmuscle type B	R.QLHLEGAS*LELS*DDDTESK.T	S1952S1956*	HPRD:01178_1	0.017049285	3.38772E-05	3	*MYH10*	01178_1
Myosin heavy chain, nonmuscle type B	R.GGPISFS*SSR.S	S1937	HPRD:01178_1	0.047808617	2.16877E-05	2	*MYH10*	01178_1
Paxillin	R.FIHQQPQS*SSPVYGSSAK.T	S83*	HPRD:03937_1	0.074088561	0.000279604	3	*PXN*	03937_2
Erythrocyte membrane protein band 4.1	R.LFS*SFLK.R	S84	HPRD:00558_1	0.104031741	1.76077E-05	2	*EPB41*	00558_2
Erythrocyte membrane protein band 4.1	R.LFSS*FLK.R	S85	HPRD:00558_1	0.104031741	1.76077E-05	2	*EPB41*	00558_2
MAP3K7	R.S*IQDLTVTGTEPGQVS*SR.S	S439S454*	HPRD:04011_1	0.108429364	0.000178486	2	*MAP3K7*	04011_4
Myosin heavy chain, nonmuscle type B	R.QLHLEGASLELS*DDDTESK.T	S1956*	HPRD:01178_1	0.113452724	0.000402341	3	*MYH10*	01178_1
ERK2	R.VADPDHDHTGFLT* EY*VATR.W	T185Y187*	HPRD:01496_1	0.128708662	7.37351E-05	3	*MAPK1*	01496_2
SHC (Src homology 2 domain containing) transforming protein 1	R.ELFDDPSY*VNVQNLDK.A	Y427*	HPRD:02780_1	0.15029448	0.000762219	2	*SHC1*	02780_2
Williams Beuren syndrome chromosome region 1	R.AYS*SFGGGRGSR.G	S13*	HPRD:11940_1	0.163809196	5.6494E-05	3	*EIF4H*	11940_2
Zyxin	R.S*PGAPGPLTLK.E	S344*	HPRD:03592_1	0.193649965	2.9433E-05	2	*ZYX*	03592_2
Erythrocyte membrane protein band 4.1	K.IEVKEES*PQS*KAETELK.A	S188S191	HPRD:00558_1	0.196565066	7.81528E-07	3	*EPB41*	00558_2
Filamin A, alpha	K.AFGPGLQGGS*AGSPAR.F	S1081*	HPRD:02060_1	0.225995795	4.14801E-07	2	*FLNA*	02060_1

(*continued*)

TABLE 1. (CONTINUED)

Protein name	*Peptide sequence (*phosphorylated, #methionine oxidation)*	*Phosphorylation site (p-site)*	*Accession no. for p-site*	*Ratio K562-STI-R/K562*	*q-Values*	*Charge state*	*Gene symbol*	*HPRD accession*
Myc proto-oncogene protein	M.PLNVS*FTNR.N	S6	UNI:P01106	0.229391119	0.00011783	2	*MYC*	
Erythrocyte membrane protein band 4.1	R.LST*HSPFR.T	T710*	HPRD:00558_1	0.238296778	0.000122817	2	*EPB41*	00558_4
SOS1	R.DGPPLLENAHS*S.-	S1332	HPRD:01681_1	0.238884192	2.45255E-05	2	*SOS1*	01681_1
CRK	R.LLDQQNPDEDFS*.-	S304	HPRD:01267_1	0.256892592	5.84008E-06	2	*CRK*	01267_1
Filamin A, alpha	K.AFGPGLQGGSAGS*PAR.F	S1084*	HPRD:02060_1	0.320034539	0.002956223	2	*FLNA*	02060_1
MAP3K7	R.S*IQDLTVTGTEPGQVSSR.S	S439*	HPRD:04011_1	0.374568908	2.26197E-05	2	*MAP3K7*	04011_4
MAP2K2	R.LNQPGT*PTR.T	T394*	HPRD:03164_1	0.40428212	2.40617E-05	2	*MAP2K2*	03164_1
MAP3K7	R.SIQDLTVT*GTEPGQVSSR.S	T446*	HPRD:04011_1	0.459359346	0.000797977	3	*MAP3K7*	04011_4
MAP3K7	R.SIQDLTVTGT*EPGQVSSR.S	T448*	HPRD:04011_1	0.46011863	0.000781265	3	*MAP3K7*	04011_4
MAP3K7	R.SIQDLT*VTGTEPGQVSSR.S	T444*	HPRD:04011_1	0.462145995	0.000747788	3	*MAP3K7*	04011_4
EIF4G3	R.S*PVPAQIAITVPK.T	S495*	HPRD:06802_1	0.524468385	0.037236161	2	*EIF4G3*	06802_1
Zyxin	K.LGHPEALSAGTGS* PQPPSFTYAQQR.E	S308*	HPRD:03592_1	0.537300804	0.016351316	3	*ZYX*	03592_2
c-Myc	K.KFELLPT*PPLS*PSRR.S	T73S77*	HPRD:01818_1	0.58647132	0.019836997	3	*MYC*	01818_1
Nucleolin	R.LELQGPRGS*PNAR.S	S563*	HPRD:01245_1	1.333398242	0.001838834	2	*NCL*	01245_1
Nucleolin	K.KVVVS*PTKK.V	S67*	HPRD:01245_1	1.506374651	0.00264531	2	*NCL*	01245_1
Nucleolin	K.KVVVSPT*KK.V	T69*	HPRD:01245_1	1.506374651	0.00264531	2	*NCL*	01245_1
Nucleolin	K.GFGFVDFNS*EEDAK.A	S619*	HPRD:01245_1	1.601309703	0.014442235	2	*NCL*	01245_1
Nucleolin	K.ALVAT*PGKK.G	T121*	HPRD:01245_1	1.796823121	0.024897338	2	*NCL*	01245_1
Myosin heavy chain 9, nonmuscle	R.KGAGDGS*DEEVDGK ADGAEAKPAE.-	S1943*	HPRD:01177_1	2.202907542	0.000407614	4	*MYH9*	01177_1
Myosin regulatory light chain MRLC2	R.ATS*NVFAMFDQSQIQEFK.E	S20	HPRD:10095_1	2.396215105	0.048226977	2	*MYL12A*	17619_2
ERK 1/2 signaling pathway								
MAP3K7	R.S*IQDLTVTGTEPGQVS*SR.S	S439S454*	HPRD:04011_1	0.108429364	0.000178486	2	*MAP3K7*	04011_4
Protein kinase C, beta 1	R.HPPVLT*PPDQEVIR.N	T641*	HPRD:01499_1	0.123333002	1.75336E-05	3	*PRKCB*	01499_1
ERK2	R.VADPDHDHTGFLT* EY*VATR.W	T185Y187*	HPRD:01496_1	0.128708662	7.37351E-05	3	*MAPK1*	01496_2
SHC (Src homology 2 domain containing) transforming protein 1	R.ELFDDPSY*VNVQNLDK.A	Y427*	HPRD:02780_1	0.15029448	0.000762219	2	*SHC1*	02780_2
SOS1	R.DGPPLLENAHS*S.-	S1332	HPRD:01681_1	0.238884192	2.45255E-05	2	*SOS1*	01681_1
MAP3K7	R.S*IQDLTVTGTEPGQVSSR.S	S439*	HPRD:04011_1	0.374568908	2.26197E-05	2	*MAP3K7*	04011_4
MAP2K2	R.LNQPGT*PTR.T	T394*	HPRD:03164_1	0.40428212	2.40617E-05	2	*MAP2K2*	03164_1
MAP2K2	R.LNQPGT*PTR.T	T394*	HPRD:03164_1	0.40428212	2.40617E-05	2	*MAP2K2*	03164_1
MAP3K7	R.SIQDLTVT*GTEPGQVSSR.S	T446*	HPRD:04011_1	0.459359346	0.000797977	3	*MAP3K7*	04011_4

(*continued*)

TABLE 1. (CONTINUED)

Protein name	*Peptide sequence (*phosphorylated, #methionine oxidation)*	*Phosphorylation site (p-site)*	*Accession no. for p-site*	*Ratio K562-STI-R/K562*	*q-Values*	*Charge state*	*Gene symbol*	*HPRD accession*
MAP3K7	R.SIQDLTVTGT*EPGQVSSR.S	T448*	HPRD:04011_1	0.46011863	0.000781265	3	*MAP3K7*	04011_4
MAP3K7	R.SIQDLT*VTGTEPGQVSSR.S	T444*	HPRD:04011_1	0.462145995	0.000747788	3	*MAP3K7*	04011_4
MAP3K8	R.NIGS*DFIPR.G	S141	HPRD:01863_1	2.471643237	0.000126802	2	*MAP3K8*	01863_1
Protein kinase C delta	R.AS*TFCGTPDYIAPEILQGLK.Y	S506*	HPRD:01501_1	6.324500473	0.014223	3	*PRKCD*	01501_2
Transport–the role of APV in regulation of aquaporin								
Protein kinase, cAMP dependent, regulatory type II, alpha	R.VADAKGDS*ES* EEDEDLEVPVPSR.F	S78S80*	HPRD:01484_1	0.058727412	2.57063E-05	2	*PRKAR2A*	01484_1
Protein kinase, cAMP dependent, regulatory type II, alpha	K.MFGS*SVDLGNLGQ.-	S395	HPRD:01484_1	0.08484677	0.001111705	2	*PRKAR2A*	01484_1
Synaptosomal-associated protein, 23 kd	K.TTWGDGGENS*PCNVVSK.Q	S110	HPRD:03962_1	0.141129472	0.000102945	2	*SNAP23*	03962_1
Protein kinase, cAMP dependent, regulatory, type II, beta	R.RAS*VCAEAYN PDEEEDDAESR.I	S114*	HPRD:01486_1	0.290252792	9.12088E-05	3	*PRKAR2B*	01486_1
Protein kinase, cAMP dependent, regulatory, type I, alpha	R.TDSREDEIS*PPPPNPVVK.G	S83*	HPRD:01786_1	0.51476936	0.011064665	3	*PRKAR1A*	01786_3
Guanine nucleotide-binding protein G(S), alpha subunit	R.ISTAS*GDGR.H	S995	HPRD:00761_1	3.921542175	0.000408155	2	*GNAS*	00761_6
Development–negative regulation of HIPPO and positive regulation of YAP/TAZ								
LIMD1	R.SS*EGSLGGQNSGIGGR.S	S240	HPRD:05177_1	0.038093765	0.000219693	2	*LIMD1*	05177_1
Rho guanine nucleotide exchange factor 2	R.QSLLGS*R.R	S137	HPRD:10458_1	0.087942015	0.020979399	2	*ARHGEF2*	10458_2
Rho guanine nucleotide exchange factor 2	K.NNTALQSVS*LR.S	S109	HPRD:10458_1	0.21884569	0.00040601	2	*ARHGEF2*	10458_2
Rho guanine nucleotide exchange factor 2	R.S*LPAGDALYLSFNPPQPSR.G	S885*	HPRD:10458_1	0.22363664	0.003435839	3	*ARHGEF2*	10458_2
LATS1	R.SNS*FNNPLGNR.A	S464*	HPRD:09147_1	0.251673373	0.000262497	2	*LATS1*	09147_1
LATS1	K.QIT*TSPITVR.K	T611*	HPRD:09147_1	0.26611696	7.89302E-06	2	*LATS1*	09147_1
Ring finger protein 131	K.SSAGDTEFVHQNS*QEIQR.S	S253	HPRD:11436_1	0.266846173	0.000795098	3	*PJA2*	11436_1
Rho guanine nucleotide exchange factor 2	R.EPALPLEPDSGGNT* SPGVTANGEAR.T	T694*	HPRD:10458_1	0.30272125	0.000207263	3	*ARHGEF2*	10458_2
Rho guanine nucleotide exchange factor 2	R.EPALPLEPDS* GGNTSPGVTANGEAR.T	S690*	HPRD:10458_1	0.303583488	0.000208202	3	*ARHGEF2*	10458_2

(*continued*)

TABLE 1. (CONTINUED)

Protein name	*Peptide sequence (*phosphorylated, #methionine oxidation)*	*Phosphorylation site (p-site)*	*Accession no. for p-site*	*Ratio K562-STI-R/K562*	*q-Values*	*Charge state*	*Gene symbol*	*HPRD accession*
Bromodomain adjacent to zinc finger domain, 1B	R.SDVQEES*EGSDT*DDNKDS AAFEDNEVQDEFLEK.L	S705T710*	HPRD:10416_1	0.328193897	0.002398843	4	*BAZ1B*	10416_3
Bromodomain adjacent to zinc finger domain, 1B	R.SDVQEES*EGSDTDDNKDS* AAFEDNEVQDEFLEK.L	S705S716*	HPRD:10416_1	0.328193897	0.002398843	4	*BAZ1B*	10416_3
BAZ2A	R.AGDPGEMPQS*PTGLGQPK.R	S1397*	HPRD:10417_1	0.374052449	0.005143065	2	*BAZ2A*	10417_1
WW domain-containing transcription regulator protein 1 (Fragment)	R.KGPS*M#LGK.L	S13	UNI:H7C4Z7	0.380989775	0.004328685	2	*WWTR1*	
ARHGEF11	R.NSVLSDPGLDSPRT*S* PVIMAR.V	T294S295*	HPRD:09302_1	0.430525392	0.002227269	3	*ARHGEF11*	09302_2
Bromodomain adjacent to zinc finger domain 1A	R.KRQS*PEPSPVTLGR.R	S1531*	HPRD:12034_1	0.545102594	0.000565312	3	*BAZ1A*	12034_3
Bromodomain adjacent to zinc finger domain, 1B	K.SLS*GSPLK.V	S347	HPRD:10416_1	0.588509068	0.001764533	2	*BAZ1B*	10416_3
Bromodomain adjacent to zinc finger domain, 1B	K.SLSGS*PLK.V	S349	HPRD:10416_1	0.592427318	0.002032571	2	*BAZ1B*	10416_3
LIM domain containing 2	R.SKS*FSLR.A	S29	HPRD:14407_1	24.16883591	1.33096E-05	2	*LIMD2*	14407_1

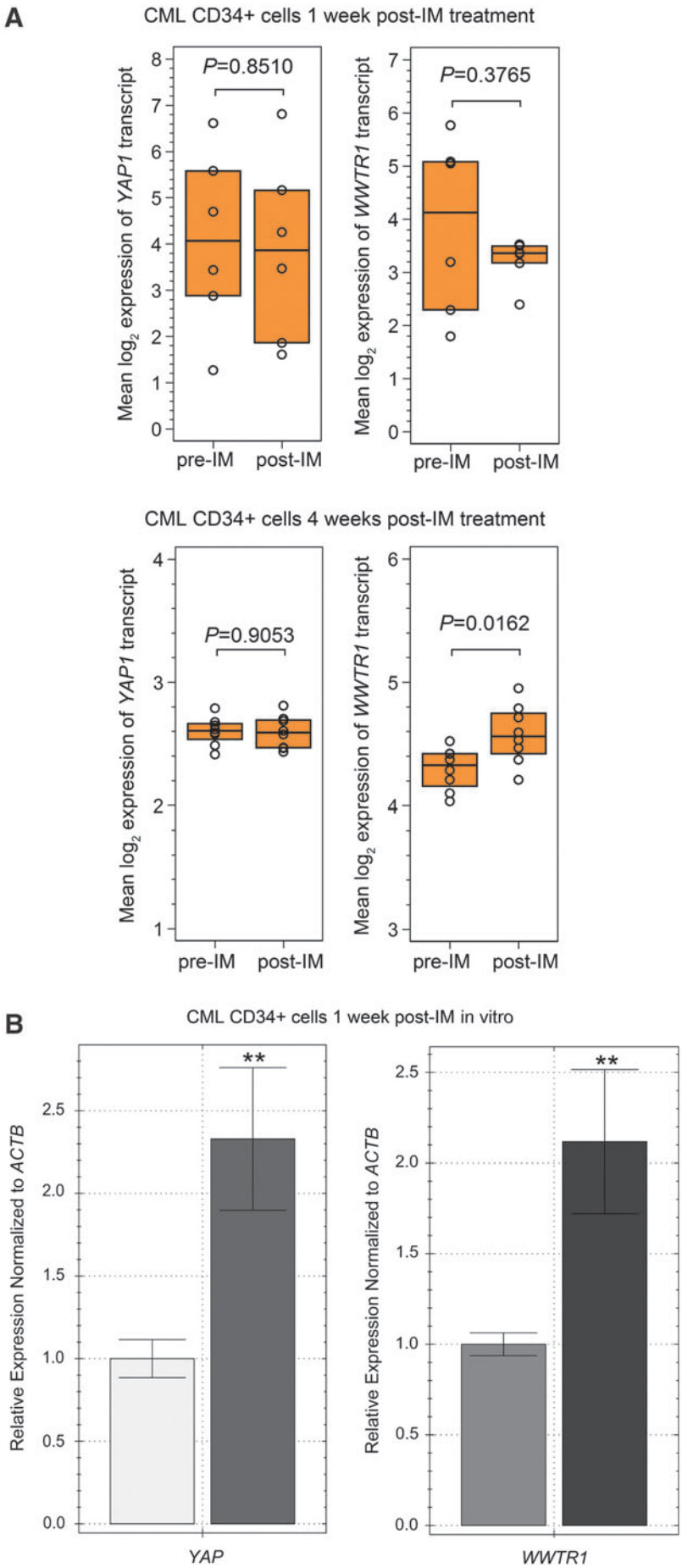

FIG. 4. The effect of IM exposure on expression of *YAP1* and *WWTR1* (*TAZ*) **(A)** Affymetrix Human Genome U219 Array data were used to examine *YAP1* and *WWTR1* (TAZ) transcript expression. $CD34^+$ cells obtained from the bone marrow of CML patients at diagnosis ($n=6$, pre-IM) and 1 week after the initiation of therapy ($n=6$, post-IM), and at diagnosis ($n=9$, pre-IM) and 4 weeks after the initiation of therapy ($n=9$, post-IM). The following probe sets were evaluated in GEO GSE12211 and GSE33075 213342_at for *YAP1* and 202134_s_at for *WWTR (TAZ)1,* expression of the probes is presented as interquartile range and median of normalized, log-transformed raw data. *P*-values are denoted on the graphs. **(B)** *YAP* and *WWTR1* expression in CML $CD34^+$ cells cultured in the presence of 5 μM IM was determined. CML $CD34^+$ cells were obtained from the bone marrow of three CML patients prior initiation of TKI therapy. Normalized expression relative to *ACTB* expressed as fold change, is presented. Samples were cultured and run in triplicate. Representative data from three independent analyses are shown $^{**}P<0.01$.

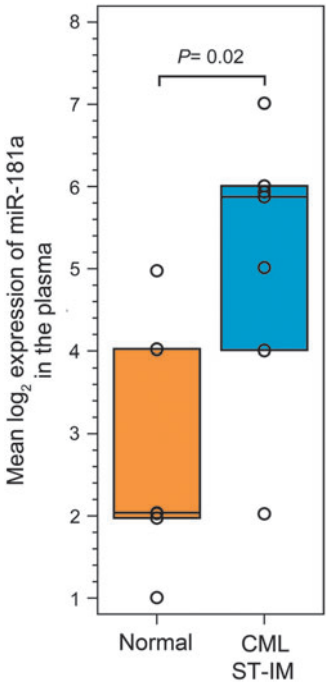

FIG. 5. Effect of long-term exposure to IM on levels of miR-181a. Taqman Human MicroRNA A (Card v2.0) Array data were used to examine miR-181a expression in unselected CML patients from the STOP-IM group ($n=7$) and 7 healthy volunteers ($n=7$). The hsa-miR-181a-4373117 probe set data were extracted from the GEO GSE75392 (platform GPL13987) data set. The geometric mean of normalized, log-transformed raw data is presented. *P*-value is denoted on the graph.

inactivation of Hippo signaling and increased activation of YAP/TAZ.

Long-term exposure to IM results in increased levels of miR-181a in the plasma of CML patients

We have previously shown that K562 CML cells subjected to prolonged exposure to IM exhibit a decrease in Bcr-Abl1 protein and activity while maintaining high Akt/Erk 1/2 signaling, enhanced proliferation, and an adhesive phenotype ([29] and Supplementary Fig. S2). MicroRNA profiling of these cells indicated significant downregulation of miR-663b and -4726, and upregulation of miR-181a, -182, -183, -438a, -513a, -847–1587, -4537, 4539, and -4690 [29]. We focused our subsequent studies on miR-181a as miR-181 family is the most highly conserved and the most preferentially expressed in the hematopoietic system [22,23]. To explore the association of miR-181a upregulation with long-term exposure to IM, we analyzed a published microarray data set: GEO GSE75392; seven CML patients from STOP-IM group and seven healthy volunteers [30]. We found that miR-181a was significantly upregulated in plasma isolated from CML STOP-IM group patients (Fig. 5). These data, which correspond to our published findings, are consistent with an association of miR-181a overexpression with prolonged exposure to IM. We, therefore, pursued studies to investigate the functional significance of these changes.

Inhibition of miR-181a does not significantly affect proliferation or apoptosis

Upregulation of one of the micro RNAs from miR-181a family, miR-181c, was recently shown to inactivate the Hippo pathway, leading to hyperactivation of YAP/TAZ and chemoresistance in pancreatic cancer [47]. Interestingly, upregulation of the stem cell transcription factor *SOX2* antagonizes the Hippo pathway leading to exaggerated YAP function [48]. The upregulation of miR-181a and *SOX2* transcripts that we observed in K562-STI-R cells, and the positive regulation of YAP in these cells, indicated a mechanistic relationship between these elements. To elucidate that relationship, we designed a miR-181a sponge inhibitor according to the method established by Kluiver et al. [49] (Fig. 6A). Effectiveness of the sponge was evaluated by measuring the intracellular levels of miR-181a transcript by RT-PCR. The miR-181a sponge induced a 50% percent decrease in miR-181a transcript levels (Fig. 6B). As we had already shown that miR-181a targets the 3′ untranslated region of *ABI1* (positions 131–137) [29], we quantified *ABI1* transcript levels by RT-PCR. In K562-STI-R cells expressing the miR181a sponge, we observed a nearly 35% increase in *ABI1* mRNA levels accompanied by an increase in Abi-1 protein levels (Supplementary Fig. S6A, B). To analyze the impact of miR-181a inhibition on cell proliferation and apoptosis, we evaluated the number of cells electroporated with a control sponge or with the miR-181a sponge, and the percentage of phosphatidylserine exposing early apoptotic cells at 24 h after electroporation. We noted no significant effect of miR-181a inhibition on proliferation or apoptosis (Fig. 6C, D). Electroporation efficiency in K562-STI-R cells was 50–55% as evaluated by FACS (Supplementary Fig. S7).

Inhibition of miR-181a results in decreased expression of stem cell markers SOX2 *and* SALL4 *and negatively regulates YAP*

To test the hypothesis that overexpression of miR-181a is associated with increased expression of the *SOX2* and *SALL4* stem cell markers, we evaluated the effect of miR-181a inhibition on the transcript levels of these genes using RT-PCR. We observed a negative effect of miR-181a inhibition on the expression of SOX2 and SALL4 (Fig. 7A), with transcript levels decreased by 20% and 30%, respectively, in K562-STI-R cells expressing the miR-181a sponge. Inhibition of miR-181a had no effect on the expression of adhesion receptors measured by FACS (Fig. 7B). Examination of the effect of miR-181a inhibition on the Hippo pathway showed positive effect on phosphorylation of YAP on Ser 127 and 397 and a decrease in the levels of YAP protein (Fig. 7C). Evaluation of the effect of miR-181a inhibition on cellular localization of YAP showed its preferential nuclear and perinuclear localization in K562-STI-R cells electroporated with control sponge, and increased cytoplasmic sequestration of YAP in K562-STI-R cells electroporated with miR-181a sponge (Fig. 7D). No actin stress fibers were observed in adherent K562-STIR cells and no significant effect of the miR-181a inhibition on cell shape and spreading was observed (Fig. 7E). Inhibition of miR-181a was associated with downregulation of the YAP target

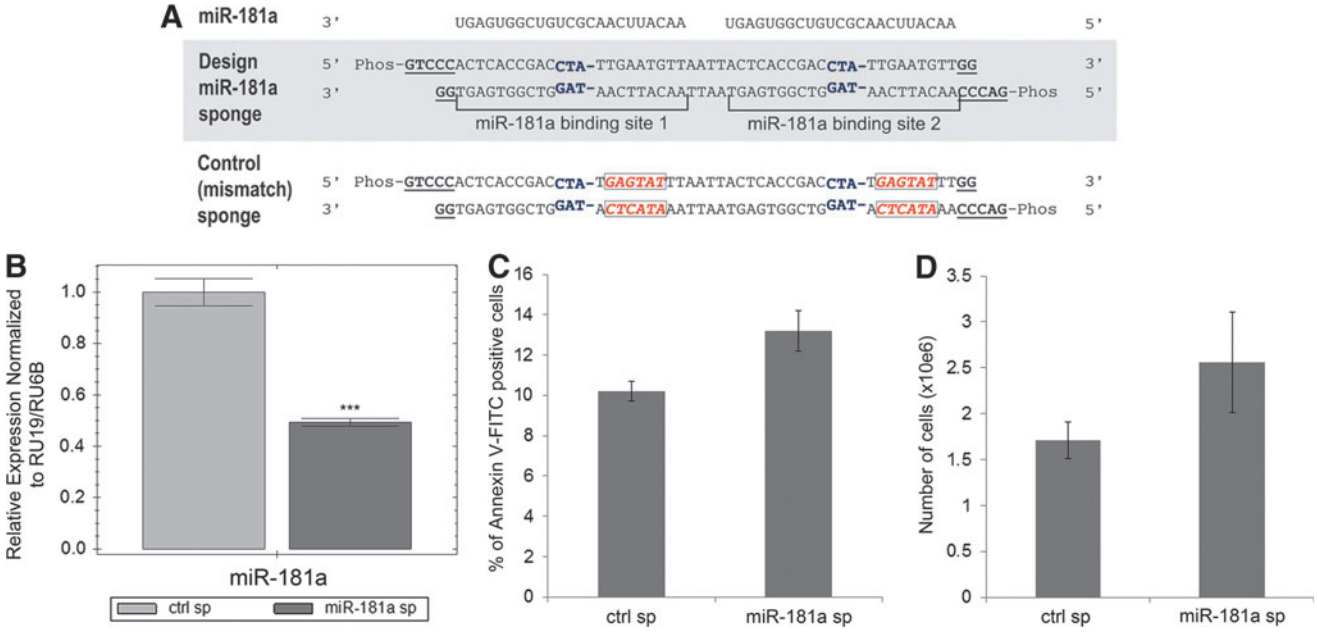

FIG. 6. The effects of an miR-181a sponge inhibitor on IM-resistant K562-STI-R cells. **(A)** Schematic representation of the miR-181a sponge and the control sponge. The central mismatch at positions 11–14 (in which the nucleotide at position 14 was deleted) in each miRNA-binding site is shown in *blue*. The scrambled sequence for the control sponge is shown in *red*. Overhangs compatible with the restriction endonuclease SanDI are shown in *underlined*, *bold* font. **(B)** RT-PCR analyses of the levels of miR-181a in K562-STI-R cells electroporated with the control vector or that encoding the miR-181a sponge inhibitor. Expression relative to RU19 and RU6B is shown as fold difference. Triplicate analyses representative of data from three independent experiments are shown. ***$P < 0.001$ **(C)** FACS analyses of the percentage of apoptotic, Annexin V-FITC-positive K562-STI-R cells electroporated with the control vector or the miR-181a sponge inhibitor. Data represent four independent experiments. **(D)** K562-STI-R cells electroporated with the control vector or the miR-181a sponge inhibitor were cultured for 24 h. Cell count was determined. Data from three independent experiments are presented.

gene *CTGF* (Fig. 7F). We also evaluated the effect of miR-181a inhibition on responsiveness to IM treatment. K562-STI-R cells that expressed the miR-181a-inhibiting sponge showed modest, but significant increase in their sensitivity to IM treatment (Fig. 7G), indicating that inhibition of miR-181a may at least partially restore sensitivity to IM. In sum, these data suggest that inhibition of miR-181a can contribute to a decrease in the expression of stem cell markers and downregulation of YAP activity, consistent with a regulatory function of miR-181a in Hippo/YAP signaling and, ultimately, the adaptation of CML cells to tonic TKI exposure.

Discussion

It is estimated that about 40% of patients who remain on IM for more than 5 years will achieve the status of *undetectable minimal residual disease* (UMRD), as defined by undetectable levels of *BCR-ABL1* transcript in peripheral blood, and that 40% of those with UMRD will remain in MR upon TKI discontinuation [7]. However, TKI discontinuation in patients with 2-year UMRD resulted in a 53% rate of relapse within the first 4 months of stopping IM [7]. These and similar studies [6,10,50] demonstrate that TKI therapy is not able to eradicate CML-initiating cells, and that the measurement of *BCR-ABL1* transcript levels in peripheral blood may not be the optimal criterion for treatment discontinuation. It is thought that rare LS/PCs that are insensitive to TKI therapy may be the cause of relapse [5,7]. At the same time, accumulating evidence points to a paradoxical involvement of TKI in induction of the stem cell phenotype and promotion of an adhesion-dependent phenotype [11,12,29].

We interpret our data as providing support for the emerging concept of therapy-dependent selection for cells, which, by upregulating certain clusters of markers typically associated with the stem cell phenotype and cell plasticity, are able to survive in the presence of the chemotherapeutic insult and retain disease-initiating capacity. Several reports that suggest chemotherapy-induced transition to a stem cell-like state [12,47,51–54] point to the role of multidrug resistance proteins, Wnt signaling, epithelial–mesenchymal (EMT) transition, and the Hippo/YAP/TAZ pathway in the acquisition of the chemoresistance-induced stem cell phenotype [47,54,55]. In this study we show that even short exposure to IM, both in vivo and in vitro may, within a population of CML $CD34^+$ BM isolated cells, induce expression of genes such as *NOTCH1*, *STAT3*, or *CD44*. Since the population of $CD34^+$ cells contains both $CD38^-$ and $CD38^+$ fractions, a shift toward increased levels of stem cell markers may be associated with IM-induced reduction of the $CD34^+CD38^+$ population in favor of more primitive, IM-insensitive $CD34^+CD38^-$ cells. Regardless of whether IM directly induces an increase in stem cell markers or spares the population of CML stem cells, its effect of protecting cells with a stem cell phenotype seems apparent.

In our cellular model of long-term exposure to IM, both genetic and surface markers that are typically associated with the stem cell-like phenotype (*SOX2*, *SALL4*, CD44,

VLA-4, and CXCR4) are upregulated. With the goal of identifying a molecular mechanism that may be involved in the transition to a stem-like phenotype, we performed unlabeled quantitative phosphoproteomics. This approach identified the Hippo/YAP pathway as a dysregulated pathway induced by long-term IM exposure. Comparing our data to the published Hippo pathway interaction networks determined by affinity purification mass spectrometry [56,57], we were able to confirm dysregulation of 9 out of 52 Hippo core interactors and 146 out of 715 Hippo pathway

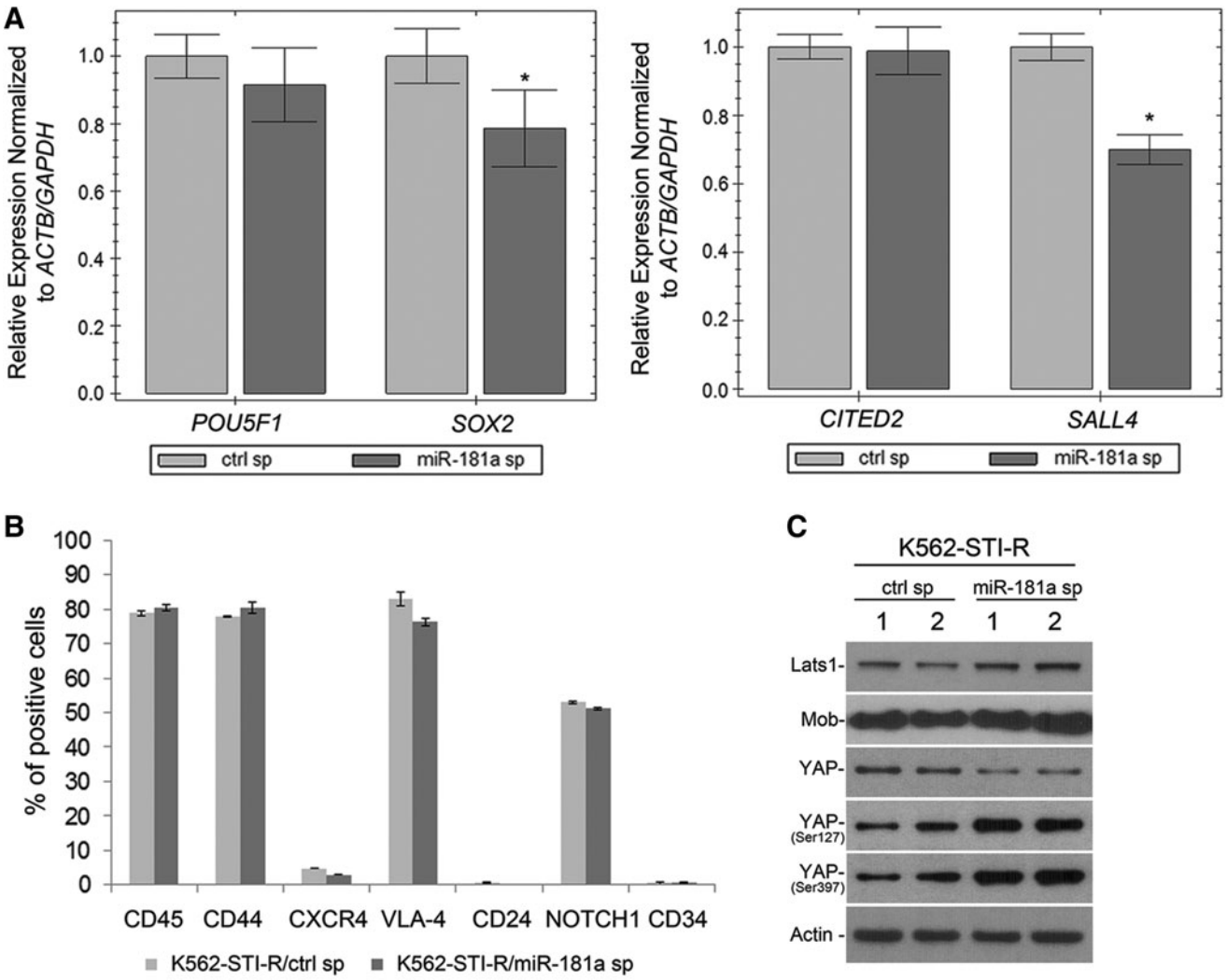

FIG. 7. Effect of miR-181a on *SOX2* and *SALL4* expression, YAP activity, and sensitivity to IM. **(A)** Analysis of expression of *POU5F1, SOX2, CITED2, and SALL4 in* K562-STI-R cells expressing the control sponge or the miR-181a sponge inhibitor. Normalized expression relative to *ACTB*, *S18*, and *GAPDH* is presented as fold difference. Triplicate analyses representing three independent experiments are shown. $*P < 0.05$ **(B)** Analyses of CD45, CD44, CXCR4, VLA-4, CD24, NOTCH1, and CD34 expression by FACS in K562-STI-R expressing the control sponge or the miR-181a sponge inhibitor. Representative data from three independent analyses are shown. **(C)** Western blot analysis was performed on the whole cell lysates prepared from K562-STI-R cells expressing the control sponge or the miR-181a sponge inhibitor. Levels of Lats1, Mob, and YAP along with phosphorylation of YAP on Ser127 and 397 were evaluated. Data from two independent electroporation reactions using control (ctrl sp: 1, 2) and miR-181a sponge (miR-181a sp: 1, 2) are presented. The results are representative of three independent experiments. Immunofluorescent analysis was performed to examine the cellular distribution of YAP **(D)** and F-actin **(E)**. K562-STI-R cells were electroporated with GFP-tagged control sponge or miR-181a sponge. Anti-YAP followed by secondary antibody conjugated with AlexaFluor 555 and phalloidin conjugated with AlexaFluor 555 were used to visualize YAP and F-Actin, respectively (*red*), and DAPI (*blue*) was used to stain the nucleus. Confocal images were acquired with a Nikon C1si confocal. Z series sections were collected at 0.2 μm with a 60× PlanApo objective. **(F)** RT-PCR analysis of *AREG, BIRC5,* and *CTGF* expression in K562-STI-R cells expressing the control sponge or the miR-181a sponge inhibitor. Normalized expression relative to *ACTB* and *GAPDH* is presented as fold difference. The triplicate analyses are representative of data from three independent experiments. $*P < 0.05$ **(G)** FACS analyses of the percentage of apoptotic cells in a population of K562-STI-R cells expressing control or miR-181a sponge inhibitor subjected to the incremental concentrations of IM. Cells 16 h after electroporation with vectors encoding the control sponge or the miR-181a sponge inhibitor were cultured for 24 h in the presence of IM. The percent of Annexin V-FITC-positive cells was determined. Representative data from three independent analyses are shown $*P < 0.05$.

(*Continued* →)

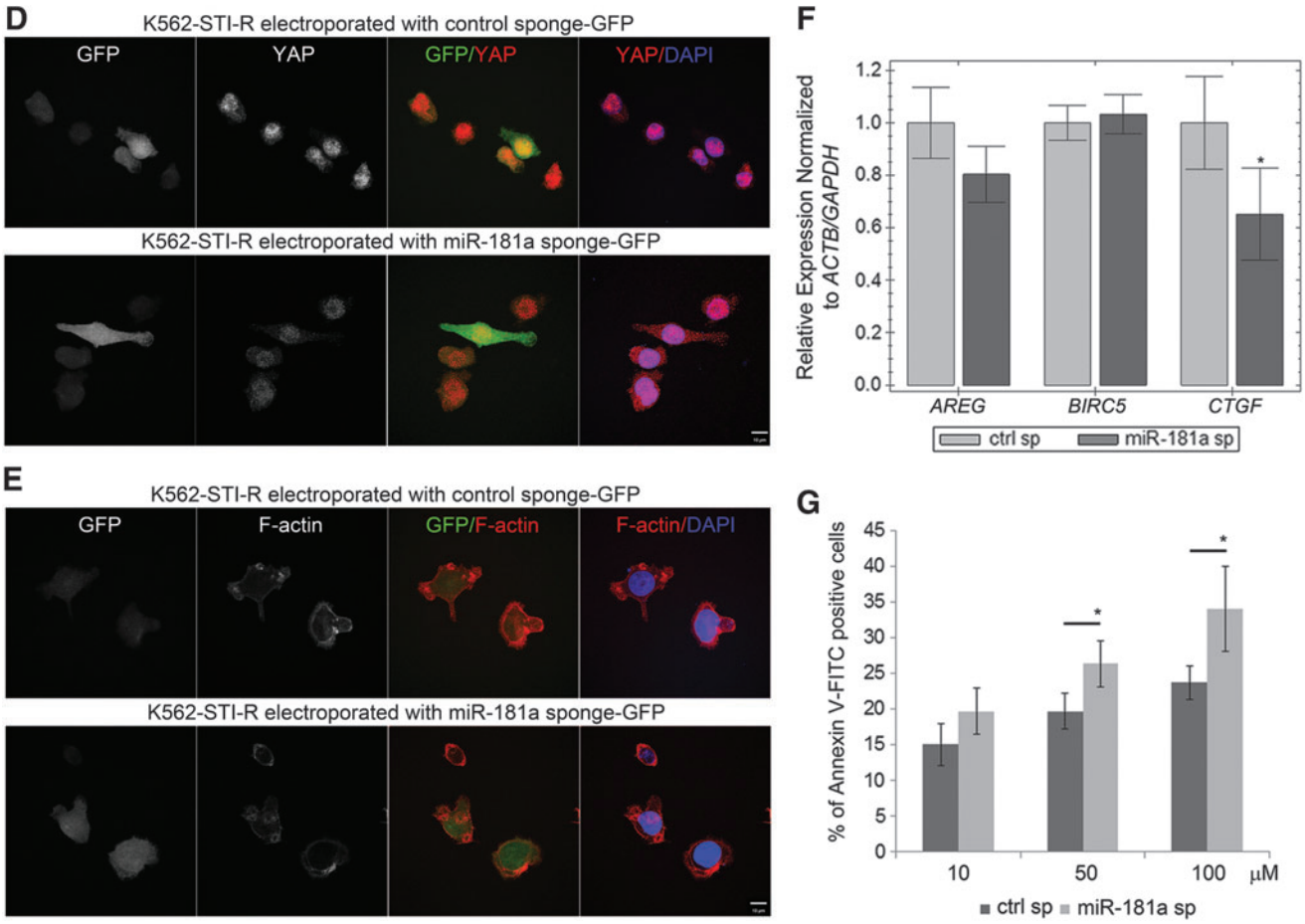

FIG. 7. (Continued).

interactors in K562-STI-R cells (Supplementary Table S2). Having seen high levels of expression of YAP and TAZ, one would expect YAP/TAZ target genes to be significantly upregulated (eg, CTGF, AREG, and BIRC5 [58–60]). The fact that we only observed increased transcript levels of CTGF may be associated with the mechanism by which YAP and TAZ regulate expression. Both translocate to the nucleus and bind to sequence-specific transcription factors TEAD1–TEAD4 and other transcription factors, such as SMAD, RUNX, TP73, TBX5, and PAX, thus enabling the transcription of target genes. That is, YAP/TAZ activity depends on the presence of other transcription factors. These other factors may be absent or inactive in IM-resistant cells.

Although we observed upregulation of *NOTCH1* in CML $CD34^+$ cells cultured in the presence of IM in vitro, we did not see the same trends in *STAT3* or *CD44* transcript levels. These markers are clearly upregulated in CML $CD34^+$ cells isolated from the bone marrow after systemic treatment with the drug. This discrepancy may indicate involvement of the microenvironment or the bone marrow stroma in regulation of the expression of these stem cell markers.

The Hippo pathway was first defined in *Drosophila melanogaster*. It is crucial for tissue homeostasis, cell proliferation, development, and stem cell renewal [61]. It has recently been recognized to have a role in cancer and chemoresistance [55,62]. Although the core Hippo pathway has been characterized, the regulatory mechanisms that affect this signaling cascade are poorly understood. Recent reports point to a role of miR-181 in the negative regulation of Hippo signaling resulting in hyperactivity of YAP and accrual of chemoresistance [47].

The role of miR-181 in malignant hematopoiesis remains unclear. In acute myeloid leukemia (AML), upregulation of miR-181a was associated with a higher complete remission rate and better survival [63,64]. In other studies, inhibition of miR-181 family members reversed a differentiation block [65]. In chronic lymphocytic leukemia (CLL), a decrease in miR-181a expression is implicated in disease pathogenesis [66]. miR-181a was also shown to be downregulated in del17p-CLL, an ultra high-risk subtype of CLL, and upregulated in a subset of trisomy 12-associated CLL [67]. Conflicting results have been reported regarding the role of miR-181a in CML. Some reports show low levels of miR-181a in CML cells [68,69], whereas other reports show increased levels of miR-181a in CML blast crises [70]. Taken together, these studies support a role for miR-181 in leukemogenesis. Inconsistencies in its reported expression levels may be a result of the genetic and cytogenetic complexity of these malignancies as well as variation in cell sources (peripheral blood vs. bone marrow) and cell types.

Given the significant miR-181a upregulation in plasma of IM-exposed CML patients and in K562-STI-R cells, and the significant increase in levels of YAP, we reasoned that this microRNA may be involved in the regulation of Hippo pathway activity. Indeed, direct and specific inhibition of

miR-181a resulted in downregulation of YAP levels along with decreases in *SOX2* and *SALL4* transcripts. Furthermore, miR-181a inhibition was associated with an increase in responsiveness to IM. However, it should be noted that the observed effect of miR-181a inhibition, while significant, remains relatively modest. This may reflect a high degree of functional redundancy between the members of the family, particularly miR-181a, -c, and -d.

In summary, our studies provide evidence that TKI treatment, while highly efficient in eradicating *BCR-ABL1*-positive progenitor cells, may be paradoxically involved in protecting a population of rare leukemic stem cells, and promoting or maintaining their stem cell potential. Our findings are consistent with a mechanism that involves downregulation of Hippo signaling and increased activity of the transcriptional coeffector YAP. Our observations indicate a role for miR-181a, and identify miR-181a and components of the Hippo/YAP pathway as potential targets to enhance the therapeutic effectiveness of TKIs in leukemia.

Acknowledgments

The authors thank Mandy Pereira, Mark Dooner, Elaine Pappa, Michael DelTatto, Joan Boylan, Aleksander F. Sikorski, Loren Fast, and Peter Quesenberry for helpful suggestions and technical assistance. This work was supported by a Brown Biomed Division DEANS Award grant (PMD), University of Medicine Foundation Integration Funding (PMD), Rhode Island Foundation grant (PMD), a pilot grant from the Lifespan COBRE Center for Cancer Research Development (1P30GM110759-01A) (PMD), Savit Foundation (PMD), and R01HL121796 (DT). AJO is supported by the American Society of Hematology Research Scholar award.

Author Disclosure Statement

No competing financial interests exist.

References

1. Bower H, M Bjorkholm, PW Dickman, M Hoglund, PC Lambert and TM Andersson. (2016). Life Expectancy of Patients With Chronic Myeloid Leukemia Approaches the Life Expectancy of the General Population. J Clin Oncol 34:2851–2857.
2. Rousselot P, A Charbonnier, P Cony-Makhoul, P Agape, FE Nicolini, B Varet, M Gardembas, G Etienne, D Rea, et al. (2014). Loss of major molecular response as a trigger for restarting tyrosine kinase inhibitor therapy in patients with chronic-phase chronic myelogenous leukemia who have stopped imatinib after durable undetectable disease. J Clin Oncol 32:424–430.
3. Chomel JC, ML Bonnet, N Sorel, A Bertrand, MC Meunier, S Fichelson, M Melkus, A Bennaceur-Griscelli, F Guilhot and AG Turhan. (2011). Leukemic stem cell persistence in chronic myeloid leukemia patients with sustained undetectable molecular residual disease. Blood 118:3657–3660.
4. Chomel JC, ML Bonnet, N Sorel, I Sloma, A Bennaceur-Griscelli, D Rea, L Legros, A Marfaing-Koka, JH Bourhis, et al. (2016). Leukemic stem cell persistence in chronic myeloid leukemia patients in deep molecular response induced by tyrosine kinase inhibitors and the impact of therapy discontinuation. Oncotarget 7:35293–35301.
5. Corbin AS, A Agarwal, M Loriaux, J Cortes, MW Deininger and BJ Druker. (2011). Human chronic myeloid leukemia stem cells are insensitive to imatinib despite inhibition of BCR-ABL activity. J Clin Invest 121:396–409.
6. Mahon FX, D Rea, J Guilhot, F Guilhot, F Huguet, F Nicolini, L Legros, A Charbonnier, A Guerci, et al. (2010). Discontinuation of imatinib in patients with chronic myeloid leukaemia who have maintained complete molecular remission for at least 2 years: the prospective, multicentre Stop Imatinib (STIM) trial. Lancet Oncol 11:1029–1035.
7. Ross DM, S Branford, JF Seymour, AP Schwarer, C Arthur, DT Yeung, P Dang, JM Goyne, C Slader, et al. (2013). Safety and efficacy of imatinib cessation for CML patients with stable undetectable minimal residual disease: results from the TWISTER study. Blood 122:515–522.
8. Graham SM, HG Jorgensen, E Allan, C Pearson, MJ Alcorn, L Richmond and TL Holyoake. (2002). Primitive, quiescent, Philadelphia-positive stem cells from patients with chronic myeloid leukemia are insensitive to STI571 in vitro. Blood 99:319–325.
9. Hu Y, Y Chen, L Douglas and S Li. (2009). beta-Catenin is essential for survival of leukemic stem cells insensitive to kinase inhibition in mice with BCR-ABL-induced chronic myeloid leukemia. Leukemia 23:109–116.
10. Saußele S, J Richter, A Hochhaus, FX Mahon. (2016). The concept of treatment-free remission in chronic myeloid leukemia. Leukemia 30:1638–1647.
11. Charaf L, FX Mahon, I Lamrissi-Garcia, I Moranvillier, F Beliveau, B Cardinaud, S Dabernat, H de Verneuil, F Moreau-Gaudry and A Bedel. (2017). Effect of tyrosine kinase inhibitors on stemness in normal and chronic myeloid leukemia cells. Leukemia 31:65–74.
12. Puissant A, M Dufies, N Fenouille, I Ben Sahra, A Jacquel, G Robert, T Cluzeau, M Deckert, M Tichet, et al. (2012). Imatinib triggers mesenchymal-like conversion of CML cells associated with increased aggressiveness. J Mol Cell Biol 4:207–220.
13. Beck B and C Blanpain. (2013). Unravelling cancer stem cell potential. Nat Rev Cancer 13:727–738.
14. Greaves M and CC Maley. (2012). Clonal evolution in cancer. Nature 481:306–313.
15. Takebe N, L Miele, PJ Harris, W Jeong, H Bando, M Kahn, SX Yang and SP Ivy. (2015). Targeting Notch, Hedgehog, and Wnt pathways in cancer stem cells: clinical update. Nat Rev Clin Oncol 12:445–464.
16. Yu H, H Lee, A Herrmann, R Buettner and R Jove. (2014). Revisiting STAT3 signalling in cancer: new and unexpected biological functions. Nat Rev Cancer 14: 736–746.
17. Blank U and S Karlsson. (2015). TGF-beta signaling in the control of hematopoietic stem cells. Blood 125:3542–3550.
18. Varelas X and JL Wrana. (2012). Coordinating developmental signaling: novel roles for the Hippo pathway. Trends Cell Biol 22:88–96.
19. Harvey KF, X Zhang and DM Thomas. (2013). The Hippo pathway and human cancer. Nat Rev Cancer 13:246–257.
20. Piccolo S, S Dupont and M Cordenonsi. (2014). The biology of YAP/TAZ: hippo signaling and beyond. Physiol Rev 94:1287–1312.
21. Ha M and VN Kim. (2014). Regulation of microRNA biogenesis. Nat Rev Mol Cell Biol 15:509–524.

22. Chen CZ, L Li, HF Lodish and DP Bartel. (2004). MicroRNAs modulate hematopoietic lineage differentiation. Science 303:83–86.
23. O'Connell RM and D Baltimore. (2012). MicroRNAs and hematopoietic cell development. Curr Top Dev Biol 99: 145–174.
24. Li QJ, J Chau, PJ Ebert, G Sylvester, H Min, G Liu, R Braich, M Manoharan, J Soutschek, et al. (2007). miR-181a is an intrinsic modulator of T cell sensitivity and selection. Cell 129:147–161.
25. Fu G, V Rybakin, J Brzostek, W Paster, O Acuto and NR Gascoigne. (2014). Fine-tuning T cell receptor signaling to control T cell development. Trends Immunol 35:311–318.
26. Williams A, J Henao-Mejia, CC Harman and RA Flavell. (2013). miR-181 and metabolic regulation in the immune system. Cold Spring Harb Symp Quant Biol 78:223–230.
27. Georgantas RW, 3rd, R Hildreth, S Morisot, J Alder, CG Liu, S Heimfeld, GA Calin, CM Croce and CI Civin. (2007). CD34+ hematopoietic stem-progenitor cell microRNA expression and function: a circuit diagram of differentiation control. Proc Natl Acad Sci U S A 104:2750–2755.
28. Judson RL, TS Greve, RJ Parchem and R Blelloch. (2013). MicroRNA-based discovery of barriers to dedifferentiation of fibroblasts to pluripotent stem cells. Nat Struct Mol Biol 20:1227–1235.
29. Chorzalska A, I Salloum, H Shafqat, S Khan, P Marjon, D Treaba, C Schorl, J Morgan, CR Bryke, et al. (2014). Low expression of Abelson interactor-1 is linked to acquired drug resistance in Bcr-Abl-induced leukemia. Leukemia 28:2165–2177.
30. Ohyashiki K, T Umezu, S Katagiri, C Kobayashi, K Azuma, T Tauchi, S Okabe, Y Fukuoka and JH Ohyashiki. (2016). Downregulation of Plasma miR-215 in Chronic Myeloid Leukemia Patients with Successful Discontinuation of Imatinib. Int J Mol Sci 17:570.
31. Yu K and AR Salomon. (2010). HTAPP: high-throughput autonomous proteomic pipeline. Proteomics 10:2113–2122.
32. Elias JE and SP Gygi. (2007). Target-decoy search strategy for increased confidence in large-scale protein identifications by mass spectrometry. Nat Methods 4:207–214.
33. Yu K, A Sabelli, L DeKeukelaere, R Park, S Sindi, CA Gatsonis and A Salomon. (2009). Integrated platform for manual and high-throughput statistical validation of tandem mass spectra. Proteomics 9:3115–3125.
34. Beausoleil SA, J Villen, SA Gerber, J Rush and SP Gygi. (2006). A probability-based approach for high-throughput protein phosphorylation analysis and site localization. Nat Biotechnol 24:1285–1292.
35. Demirkan G, K Yu, JM Boylan, AR Salomon and PA Gruppuso. (2011). Phosphoproteomic profiling of in vivo signaling in liver by the mammalian target of rapamycin complex 1 (mTORC1). PLoS One 6:e21729.
36. Dubielecka PM, KI Ladwein, X Xiong, I Migeotte, A Chorzalska, KV Anderson, JA Sawicki, K Rottner, TE Stradal and L Kotula. (2011). Essential role for Abi1 in embryonic survival and WAVE2 complex integrity. Proc Natl Acad Sci U S A 108:7022–7027.
37. Storey JD and R Tibshirani. (2003). Statistical significance for genomewide studies. Proc Natl Acad Sci U S A 100: 9440–9445.
38. Bruennert D, A Czibere, I Bruns, R Kronenwett, N Gattermann, R Haas and F Neumann. (2009). Early in vivo changes of the transcriptome in Philadelphia chromosome-positive CD34+ cells from patients with chronic myelogenous leukaemia following imatinib therapy. Leukemia 23:983–985.
39. Benito R, E Lumbreras, M Abaigar, NC Gutierrez, M Delgado, C Robledo, JL Garcia, AE Rodriguez-Vicente, MC Canizo and JM Rivas. (2012). Imatinib therapy of chronic myeloid leukemia restores the expression levels of key genes for DNA damage and cell-cycle progression. Pharmacogenet Genomics 22:381–388.
40. Jiang X, D Forrest, F Nicolini, A Turhan, J Guilhot, C Yip, T Holyoake, H Jorgensen, K Lambie, et al. (2010). Properties of CD34+ CML stem/progenitor cells that correlate with different clinical responses to imatinib mesylate. Blood 116:2112–2121.
41. Holtz MS, SJ Forman and R Bhatia. (2005). Nonproliferating CML CD34+ progenitors are resistant to apoptosis induced by a wide range of proapoptotic stimuli. Leukemia 19:1034–1041.
42. Boyer LA, TI Lee, MF Cole, SE Johnstone, SS Levine, JP Zucker, MG Guenther, RM Kumar, HL Murray, et al. (2005). Core transcriptional regulatory circuitry in human embryonic stem cells. Cell 122:947–956.
43. Zhang J, WL Tam, GQ Tong, Q Wu, HY Chan, BS Soh, Y Lou, J Yang, Y Ma, et al. (2006). Sall4 modulates embryonic stem cell pluripotency and early embryonic development by the transcriptional regulation of Pou5f1. Nat Cell Biol 8:1114–1123.
44. Li L and R Bhatia. (2011). Stem cell quiescence. Clin Cancer Res 17:4936–4941.
45. Al-Hajj M, MS Wicha, A Benito-Hernandez, SJ Morrison and MF Clarke. (2003). Prospective identification of tumorigenic breast cancer cells. Proc Natl Acad Sci USA 100:3983–3988.
46. McGowan PM, C Simedrea, EJ Ribot, PJ Foster, D Palmieri, PS Steeg, AL Allan and AF Chambers. (2011). Notch1 inhibition alters the CD44hi/CD24lo population and reduces the formation of brain metastases from breast cancer. Mol Cancer Res 9:834–844.
47. Chen M, M Wang, S Xu, X Guo and J Jiang. (2015). Upregulation of miR-181c contributes to chemoresistance in pancreatic cancer by inactivating the Hippo signaling pathway. Oncotarget 6:44466–44479.
48. Basu-Roy U, NS Bayin, K Rattanakorn, E Han, DG Placantonakis, A Mansukhani and C Basilico. (2015). Sox2 antagonizes the Hippo pathway to maintain stemness in cancer cells. Nat Commun 6:6411.
49. Kluiver J, I Slezak-Prochazka, K Smigielska-Czepiel, N Halsema, BJ Kroesen and A van den Berg. (2012). Generation of miRNA sponge constructs. Methods 58:113–117.
50. O'Hare T, MS Zabriskie, AM Eiring and MW Deininger. (2012). Pushing the limits of targeted therapy in chronic myeloid leukaemia. Nat Rev Cancer 12:513–526.
51. Dallas NA, L Xia, F Fan, MJ Gray, P Gaur, G van Buren, 2nd, S Samuel, MP Kim, SJ Lim and LM Ellis. (2009). Chemoresistant colorectal cancer cells, the cancer stem cell phenotype, and increased sensitivity to insulin-like growth factor-I receptor inhibition. Cancer Res 69:1951–1957.
52. Polyak K and RA Weinberg. (2009). Transitions between epithelial and mesenchymal states: acquisition of malignant and stem cell traits. Nat Rev Cancer 9:265–273.
53. Singh A and J Settleman. (2010). EMT, cancer stem cells and drug resistance: an emerging axis of evil in the war on cancer. Oncogene 29:4741–4751.
54. Touil Y, W Igoudjil, M Corvaisier, AF Dessein, J Vandomme, D Monte, L Stechly, N Skrypek, C Langlois, et al.

(2014). Colon cancer cells escape 5FU chemotherapy-induced cell death by entering stemness and quiescence associated with the c-Yes/YAP axis. Clin Cancer Res 20:837–846.
55. Zanconato F, M Cordenonsi and S Piccolo. (2016). YAP/TAZ at the Roots of Cancer. Cancer Cell 29:783–803.
56. Couzens AL, JD Knight, MJ Kean, G Teo, A Weiss, WH Dunham, ZY Lin, RD Bagshaw, F Sicheri, et al. (2013). Protein interaction network of the mammalian Hippo pathway reveals mechanisms of kinase-phosphatase interactions. Sci Signal 6:rs15.
57. Wang W, X Li, J Huang, L Feng, KG Dolinta and J Chen. (2014). Defining the protein-protein interaction network of the human hippo pathway. Mol Cell Proteomics 13:119–131.
58. Moroishi T, CG Hansen and KL Guan. (2015). The emerging roles of YAP and TAZ in cancer. Nat Rev Cancer 15:73–79.
59. Zhang J, JY Ji, M Yu, M Overholtzer, GA Smolen, R Wang, JS Brugge, NJ Dyson and DA Haber. (2009). YAP-dependent induction of amphiregulin identifies a non-cell-autonomous component of the Hippo pathway. Nat Cell Biol 11:1444–1450.
60. Liu H, D Jiang, F Chi and B Zhao. (2012). The Hippo pathway regulates stem cell proliferation, self-renewal, and differentiation. Protein Cell 3:291–304.
61. Yu FX and KL Guan. (2013). The Hippo pathway: regulators and regulations. Genes Dev 27:355–371.
62. Zhao Y and X Yang. (2015). The Hippo pathway in chemotherapeutic drug resistance. Int J Cancer 137:2767–2773.
63. Schwind S, K Maharry, MD Radmacher, K Mrozek, KB Holland, D Margeson, SP Whitman, C Hickey, H Becker, et al. (2010). Prognostic significance of expression of a single microRNA, miR-181a, in cytogenetically normal acute myeloid leukemia: a Cancer and Leukemia Group B study. J Clin Oncol 28:5257–5264.
64. Hickey CJ, S Schwind, HS Radomska, AM Dorrance, R Santhanam, A Mishra, YZ Wu, H Alachkar, K Maharry, et al. (2013). Lenalidomide-mediated enhanced translation of C/EBPalpha-p30 protein up-regulates expression of the antileukemic microRNA-181a in acute myeloid leukemia. Blood 121:159–169.
65. Su R, HS Lin, XH Zhang, XL Yin, HM Ning, B Liu, PF Zhai, JN Gong, C Shen, et al. (2015). MiR-181 family: regulators of myeloid differentiation and acute myeloid leukemia as well as potential therapeutic targets. Oncogene 34:3226–3239.
66. Marton S, MR Garcia, C Robello, H Persson, F Trajtenberg, O Pritsch, C Rovira, H Naya, G Dighiero and A Cayota. (2008). Small RNAs analysis in CLL reveals a deregulation of miRNA expression and novel miRNA candidates of putative relevance in CLL pathogenesis. Leukemia 22:330–338.
67. Visone R, LZ Rassenti, A Veronese, C Taccioli, S Costinean, BD Aguda, S Volinia, M Ferracin, J Palatini, et al. (2009). Karyotype-specific microRNA signature in chronic lymphocytic leukemia. Blood 114:3872–3879.
68. Lu J, G Getz, EA Miska, E Alvarez-Saavedra, J Lamb, D Peck, A Sweet-Cordero, BL Ebert, RH Mak, et al. (2005). MicroRNA expression profiles classify human cancers. Nature 435:834–838.
69. Wang G, R Zhao, X Zhao, XI Chen, D Wang, Y Jin, XI Liu, CI Zhao, Y Zhu, et al. (2015). MicroRNA-181a enhances the chemotherapeutic sensitivity of chronic myeloid leukemia to imatinib. Oncol Lett 10:2835–2841.
70. Machova Polakova K, T Lopotova, H Klamova, P Burda, M Trneny, T Stopka and J Moravcova. (2011). Expression patterns of microRNAs associated with CML phases and their disease related targets. Mol Cancer 10:41.

Address correspondence to:
Dr. Patrycja M. Dubielecka
Signal Transduction Lab
Division of Hematology/Oncology
Rhode Island Hospital
Warren Alpert Medical School
Brown University
One Hoppin Street
Coro West, Suite 5.01
Providence, RI 02903

E-mail: patrycja_dubielecka-szczerba@brown.edu

Received for publication September 1, 2016
Accepted after revision January 17, 2017
Prepublished on Liebert Instant Online January 19, 2017